Published in final edited form as:
Biochem Pharmacol. 2016 March 15; 104: 29–41. doi:10.1016/j.bcp.2016.01.011.

Activation of the MAPK/Akt/Nrf2-Egr1/HO-1-GCLc axis protects MG-63 osteosarcoma cells against 15d-PGJ$_2$-mediated cell death

Chintan N. Koyani[a], **Kerstin Kitz**[a,b,1], **Christine Rossmann**[a,2], **Eva Bernhart**[a], **Evelyn Huber**[b], **Christopher Trummer**[a], **Werner Windischhofer**[b], **Wolfgang Sattler**[a], and **Ernst Malle**[a,*]

[a]Institute of Molecular Biology and Biochemistry, Medical University of Graz, Graz, Austria

[b]Department of Pediatrics and Adolescence Medicine, Research Unit of Osteological Research and Analytical Mass Spectrometry, Medical University of Graz, Graz, Austria

Abstract

Despite considerable efforts to improve treatment modalities for osteosarcoma (OS), patient survival remains poor mainly due to pro-survival pathways in OS cells. Among others, prostaglandins (PGs) are the potent regulators of bone homoeostasis and OS pathophysiology. Therefore, the present study aimed to elucidate the impact of 15-deoxy-$\Delta^{12,14}$-PGJ$_2$ (15d-PGJ$_2$, a stable PGD$_2$ degradation product) on cell death/cell survival pathways in p53-deficient MG-63 OS cells. Our findings show that 15d-PGJ$_2$ induces generation of reactive oxygen species that promote p38 MAPK activation and subsequent Akt phosphorylation. This pathway induced nuclear expression of Nrf2 and Egr1, and increased transcription of haem oxygenase-1 (HO-1) and the catalytic subunit of glutamate cysteine ligase (GCLc), catalysing the first step in GSH synthesis. Silencing of Nrf2, Egr1 and HO-1 significantly elevated 15d-PGJ$_2$-mediated reduction of cellular metabolic activity. Activation of cell survival genes including HO-1 and GCLc inhibited 15d-PGJ$_2$-induced cleavage of pro-caspase-3 and PARP. Annexin V/propidium iodide staining showed an increase in early/late apoptotic cells in response to 15d-PGJ$_2$. The observed 15d-PGJ$_2$-mediated signalling events are independent of PGD$_2$ receptors (DP1 and DP2) and PPARγ. In addition, the electrophilic carbon atom C9 is a prerequisite for the observed activity of 15d-PGJ$_2$. The present data show that the intracellular redox imbalance acted as a node and triggered both death and survival pathways in response to 15d-PGJ$_2$. Pharmacological or genetic interference of the pro-survival pathway, the p38 MAPK/Akt/Nrf2-Egr1/HO-1-GCLc axis, sensitizes MG-63 cells towards 15d-PGJ$_2$-mediated apoptosis.

Keywords

15d-PGJ$_2$; Chemotherapy; PI3K/Akt axis; Peroxisome proliferator-activated-receptor γ; Pro-survival signalling; ROS; Tumour protein p53

*Corresponding author at: Institute of Molecular Biology and Biochemistry, Medical University of Graz, Harrachgasse 21, 8010 Graz, Austria. ernst.malle@medunigraz.at (E. Malle) .
[1]Present address: Fresenius Kabi Austria GmbH, Graz, Austria.
[2]Present address: Institute of Physiological Chemistry, Medical University of Graz, Graz, Austria.

Competing financial interests
The authors declare no competing financial interests.

1. Introduction

Osteosarcoma (OS), a tumour of mesenchymal origin, is the most common tumour of bone. OS has a bimodal age distribution being found predominantly in the second decade of life and in elderly people. There are a variety of different types of OS tumours that are associated with varying degrees of aggressiveness. Although prognosis for OS patients has improved within last decades, the highly metastatic potential renders this sarcoma resistant to chemotherapeutic agents leading to dismal perspectives for affected patients [1].

Due to the complexity in the nature and diversity in the genetic background, the exact aetiology of OS remains not fully understood. Out of the known aetiological factors, cyclooxygenase and its metabolites, the prostaglandins (PGs), play a pivotal role during OS development and progression [2]. Among these prostanoids, pro-inflammatory PGE_2 has a predominant role in promoting tumour growth and is assumed to be the most abundant PG found in human bone metabolism and disease [3,4]. PGD_2 can affect bone metabolism by influencing both osteoclast and osteoblast functions, both cells involved in bone remodelling and in vivo fracture repair as well [3,5,6]. In osteoblasts PGD_2 stimulated calcification [7] and altered expression of RANKL and osteoprotegerin [6,8]. Furthermore, PGD_2 favoured expression of cytokines via calcium mobilization and Rho kinase [9,10], and promoted induction of heat shock proteins via the mitogen-activated protein kinase (MAPK) pathway [11,12].

However, PGD_2 has a very short half-life [13] and is either metabolized enzymatically to 13,14-dihydro-15-keto PGD_2 [14] or readily dehydrated into J series prostanoids with a α,β-unsaturated ketone in the cyclopentenone ring. In particular, 15-deoxy-$\Delta^{12,14}$-PGJ_2 (15d-PGJ_2), the final dehydration product of PGD_2 has been shown to have wide-ranging effects on various cellular systems [15,16].

15d-PGJ_2 is a potent endogenous ligand for the peroxisome proliferator-activated-receptor γ (PPARγ) (for a review see [17]) but may interact also with the PGD_2 receptors DP1 and/or DP2. 15d-PGJ_2 may modulate cell growth, viability and proliferation and may induce cell death in further consequence. In murine HL-1 cells and primary murine cardiomyocytes apoptosis was mediated via DP2 [18], while in human umbilical vein endothelial cells [19] and synoviocytes [20] 15d-PGJ_2 induced apoptosis via PPAR γ-dependent mechanisms. PPARγ-independent induction of apoptosis has been reported in human B lymphocytes and B cell lymphoma [21], human endothelial cells [22], rabbit synovial cells [23], human hepatic myofibroblasts [24] and hepatocellular carcinoma cell lines [25]. However, less information is available on receptor-mediated (PPARγ or DP1/DP2) apoptosis by 15d-PGJ_2 in osteoblastic cells including OS cells [26–28].

Cell lines routinely used as models of OS have been derived from OS tumours and are used to study the effects of growth and specific bone-active factors as well as cytokines or prostanoids on intracellular signalling cascades and apoptosis. In particular, reactive oxygen species (ROS)-sensitive signalling pathways are persistently elevated in many types of cancers. Cancer cells evolve mechanisms to protect themselves from oxidative stress and therefore may develop sophisticated adaption that essentially involves hyperactivation of

antioxidant signalling and upregulation of pro-survival molecules. Therefore, identification and modulation of survival pathways in OS cells, that may be responsible for resistance against therapeutic agents, might help to improve therapeutic outcome.

Among all the genetic aberrations occurring in OS, p53 is the most frequently mutated (80–90%) or deleted (24–49%) gene [1]. Loss of functional transcription factor p53 is associated with redox imbalance, increased oxidative stress, high mutagenesis and aggressive tumour growth [29]. 15d-PGJ_2 has been reported to have dual effects, promoting either cell survival or inducing cell death via apoptosis. The present study aimed to elucidate potential pro-survival pathways in osteoblast-like MG-63 OS cells (deficient of tumour suppressor protein p53) and to reveal whether gene silencing and pharmacological interference may shift the balance from cell survival to cell death in response to 15d-PGJ_2 treatment.

2. Materials and methods

2.1. Cell culture

MG-63, a human OS cell line (ATCC, Manassas, VA, USA), was maintained at 37 °C under 5% CO_2 in α-MEM medium (Invitrogen, Lofer, Austria) supplemented with 5% (v/v) FCS [30] and 50 μg/ml (w/v) gentamycin (Invitrogen). Cells were used between the 10th and 20th passage counted from the day of receipt. If not otherwise stated, cells were plated at a density of 2×10^5 in 6-well plates and grown to 70% confluence [31].

2.2. Incubation protocols

MG-63 cells were treated with indicated concentrations of 15d-PGJ_2 (Cayman, MI, USA) for indicated time periods. Cells were incubated for 30 min with either an inhibitor of p38 MAPK (25 μM PD169316, Merck Biosciences, Darmstadt, Germany), *N*-acetyl-L-cysteine (NAC, 5 mM), pyrrolidine dithiocarbamate (PDTC, 1 mM), *N*-2-mercaptopropionylglycine (MPG, 5 mM) (Sigma–Aldrich, MO, USA), Tempol (1 mM, Tocris, MA, USA), PPARγ antagonist (20 μM T0070907), D-type prostanoid receptor (DP1) antagonist (100 nM MK0524), DP2 antagonist (1 μM CAY10471) (Cayman), L-buthionine-(S,R)-sulfoximine (BSO, 5 μM), GSH ethyl ester (10 mM, Sigma–Aldrich), LY294002 (10 μM) or Akt inhibitor (Akt-I, 10 μM) (Calbiochem, CA, USA) prior to 15d-PGJ_2 treatment. Alternatively, cells were treated with 9,10-dihydro-15d-PGJ_2 (dh-15d-PGJ_2, 20 μM, Cayman) for indicated time periods.

2.3. Western blot analysis

(a) Whole cell proteins—MG-63 cells were lysed in ice-cold lysis buffer (50 mM HEPES, 150 mM NaCl, 1 mM EDTA, 10 mM $Na_4P_2O_7$, 2 mM Na_3VO_4, 10 mM NaF, 1% [v/v] Triton X-100, 10% [v/v] glycerol, pH 7.4, Sigma–Aldrich) containing a protease inhibitor cocktail tablet (Roche, Vienna, Austria). Pellets were separated by centrifugation at 13,000 rpm (4 °C, 10 min).

(b) Cytosolic and nuclear proteins—For translocation experiments, nuclear and cytosolic proteins were isolated using NE-PER® Nuclear and Cytoplasmic Extraction

Reagents (Thermo Fisher Scientific, IL, USA) with additional protease inhibitors (Complete Mini protease inhibitor cocktail-tablets) according to the manufacturer's suggestions.

Protein estimation of whole cell, cytosolic and nuclear lysates was performed using BCA protein assay kit (Thermo Fisher Scientific). Whole cell (40 μg) or nuclear/cytosolic fraction (5 μg) protein lysates were added to 10 μl of NuPAGE LDS sample buffer (Invitrogen) containing 2 μl of NuPAGE sample reducing agent (Invitrogen). After heating for 10 min at 70 °C proteins were separated by electrophoresis on NuPAGE 4–12% Bis-Tris gel (Invitrogen) and transferred to nitrocellulose membranes (Invitrogen, 0.45 μm). Membranes were blocked with 5% (w/v) non-fat milk in TBST (Tris-buffered saline containing Tween 20) (25 °C, 2 h) and incubated with primary antibodies (overnight at 4 °C). The following primary antibodies (diluted in 5% [w/v] BSA-TBST) were used: anti-pp38 MAPK (1:1000 Cell Signaling-9211, MA, USA), anti-pAkt T^{308} (1:1000 Cell Signaling-4056), anti-nuclear factor (erythroid-derived 2)-like 2 protein (Nrf2) (1:1000 Santa Cruz-sc722, TX, USA), anti-early growth response-1 (Egr1) (1:1000 Santa Cruz-sc189), anti-HO-1 (1:333 Santa Cruz-sc10789), anti-glutamate cysteine ligase-catalytic subunit (GCLc, 1:200 Santa Cruz-sc166345), anti-GCL-modifier subunit (GCLm, 1:500 Santa Cruz-166603), anti-caspase-3 (1:1000 Cell Signaling-9662) or anti-Poly (ADP-ribose) polymerase (PARP) (1:1000 Biomol-SA250, Hamburg, Germany). After washing, the membranes were incubated with HRP-conjugated goat anti-mouse IgG (1:100,000 Biomol-8101102) or goat anti-rabbit IgG (1:200,000 Biomol-6293) (25 °C, 2 h). Immunoreactive bands were visualized using Super Signal West Pico Chemiluminescent substrate (Thermo Fisher Scientific) or Immobilon Western Chemiluminescent HRP substrate (Millipore, Billerica, MA, USA) and developed by Bio-Rad ChemiDoc MP Imaging System. For normalization, membranes were stripped with stripping buffer (58.4 g/L NaCl, 7.5 g/L glycine, pH 2.15, Sigma–Aldrich) and incubated with anti-p38 (1:2000 Sigma–Aldrich-M0800), anti-Akt (1:500 Santa Cruz-sc1618R), anti-Lamin (1:1000 Santa Cruz-sc20681), or anti-γ-actin antisera (1:1000 Santa Cruz-sc47778) as primary antibodies [30,32].

2.4. Annexin V/propidium iodide (PI) staining

MG-63 cells (70% confluent) were treated with 20 μM 15d-PGJ_2 up to 48 h. Cells were harvested and stained using the FITC Annexin V Apoptosis Detection Kit 1 (BD Biosciences, NJ, USA) according to the manufacturer's suggestion. Briefly, cells were washed in cold PBS and incubated with 100 μl of 1x binding buffer (containing 5 μl of Annexin V FITC and 5 μl of PI) for 15 min (25 °C) in the dark [33]. Flow cytometric analyses were performed on Guava EasyCyte 8 (Millipore, Billerica, MA, USA) and analysed using InCyte 3.1 (Millipore). To set up fluorescent compensation and gating for detection of necrosis and early/late apoptosis, unstained and single stained cells were treated with staurosporine (1 μM, 4 h, Sigma–Aldrich) or H_2O_2 (3 mM, 6 h, Herba Chemosan, Vienna, Austria).

2.5. RNA isolation and quantitative real-time PCR (qPCR)

QIAshredder and RNeasy Mini Kit (Qiagen, Hilden, Germany) were used to isolate RNA according to the manufacturer's protocol. After determining RNA concentration, one μg RNA was reverse transcribed using High-Capacity cDNA Reverse Transcription Kit

(Applied Biosystems, Foster City, CA, USA) according to the supplier's manual. For gene quantification, six ng cDNA per template was used with GoTaq qPCR Master Mix (Promega, Vienna, Austria) and gene specific primers. The qPCR protocol was performed by LightCycler 480 system (Roche Diagnostics, Vienna, Austria). The following gene specific primers were used: GAPDH (Hs_GAPDH_1_SG), Nrf2 (Hs_NFE2L2_1_SG), Egr1 (Hs_EGR1_1_SG), HO-1 (Hs_HMOX1_1_SG) and GCLc (Hs_GCLC_1_SG) (Qiagen). Relative gene expression levels were normalized to GAPDH and calculated using ΔΔCT method.

2.6. Gene silencing

MG-63 cells were transfected with siRNAs specific for Nrf2 (40 nM each, SI03246950, SI03246614, Qiagen), Egr1 (40 nM each, SI00030709, SI03052511, SI03069108, SI03078950), HO-1 (40 nM each, SI02780995, SI02780533) or scrambled negative control siRNA (40 nM si-scr; Allstars negative control siRNA, Qiagen) [18]. The siRNA transfection was performed using Lipofectamine 3000 (Invitrogen) according to the to the supplier's manual. Briefly, MG-63 cells (50% confluent) were transfected with 500 μl medium (without FCS and gentamycin) containing 3 μl of Lipofectamine 3000 and the respective siRNA for 6 h at 37 °C. Transfection medium was replaced with medium (containing FCS and gentamycin) and cells were grown for another 24 h. The mRNA expression levels of silenced genes were measured using qPCR (see above). In parallel, transfected cells were treated with 15d-PGJ_2 to follow protein expression using Western blot (see above) or cell metabolic activity using the MTT assay (see below).

2.7. Intracellular ROS measurement

Intracellular redox homoeostasis was assessed using carboxy-H_2DCFDA (5-(and -6)-carboxy-2′,7′-dichlorodihydrofluorescein diacetate, Invitrogen), a cell-permeable dye that becomes fluorescent upon oxidation by ROS. After treatment MG-63 cells were incubated with 10 μM DCFDA in PBS for 30 min at 37 °C. Cells were washed twice with ice-cold PBS and lysed with 300 μl of 3% (v/v) Triton X-100 in PBS (30 min) followed by addition of 50 μl absolute ethanol (15 min) with shaking (1350 rpm, 4 °C). Lysates were centrifuged at 10,000 rpm (4 °C, 10 min) to pellet debris. The supernatants (100 μl) were used to measure DCF (2′,7′-dichlor ofluorescein) fluorescence at emission/correction wavelengths of 485/540 nm, respectively [34]. A microtiter plate reader (Victor Multilabel Counter, Perkin-Elmer, Waltham, MA, USA) was used to measure fluorescence intensities.

2.8. Metabolic activity (MTT-reduction)

MG-63 cells (70% confluent) were treated with 15d-PGJ_2 followed by incubation with MTT (3-(4,5-dimethylthiazol-2-yl)-2,5-diphenyltetrazolium bromide) (0.5 mg/ml; dissolved in serum-free medium) for 30 min at 37 °C. The converted insoluble dark purple coloured dye (formazan) was solubilized by an addition of 300 μl acidic isopropanol (0.04 M HCl in isopropanol) [34]. Cell metabolic activity was determined by measuring optical densities at emission/correction wavelengths of 570/630 nm, respectively, by a microtiter plate reader (see above).

2.9. Glutathione assay

Intracellular glutathione was determined using a commercial Glutathione Assay Kit (Cayman) according to the manufacturer's protocol. Briefly, after treatment cells were washed twice with cold PBS and scraped in 1 ml PBS (pH 7.0) containing 1 mM EDTA. Cells were homogenized by sonication followed by deproteination with 5% metaphosphoric acid. Total GSH levels were determined according to the manufacturer's instruction and absorbance was measured at 405 nm (Multiscan® FC microplate photometer, Thermo Fisher Scientific). Absorbance values from standards and samples were subtracted with blank control values and GSH concentrations of samples were calculated by interpolation from standard curve. Results were expressed as μmoles of total GSH normalized to 10^6 cells [30].

2.10. Statistical analysis

All values are represented as mean or mean ± SEM and n represents the number of experiments. Statistical significances were tested by Student's *t*-test or a one-way ANOVA with adequate post hoc tests (Tukey or Dunett), using IBM SPSS 20 software. The *p*-values $\leqslant 0.05$ were considered statistically significant. All tests were 2-sided.

3. Results

3.1. 15d-PGJ_2 induces phosphorylation of p38 MAPK in human OS cells

As 15d-PGJ_2 has been reported to promote phosphorylation of MAPKs in various cell lines [18,30,35], we concentrated on expression of pp38 MAPK in MG-63 cells. Addition of 15d-PGJ_2 to cells induced p38 MAPK phosphorylation concentration-dependently with an adequate phosphorylation at 20 μM concentration (Fig. 1A) that is used for all further experiments. Fig. 1B shows time-dependent phosphorylation of p38 MAPK up to 30 min; maximum phosphorylation was observed from 15 min.

3.2. 15d-PGJ_2 alters intracellular redox balance

Cellular treatment by cyclopentenone PGs may induce ROS generation that co-induces alterations in intracellular signalling cascades [18,30]. To clarify whether 15d-PGJ_2 affects redox homoeostasis in MG-63 cells the redox-sensitive probe DCFDA was used. In response to 15d-PGJ_2 time-dependent increase in DCF fluorescence reached a maximum from 7.5 min with levels elevated approximately 1.7-fold over baseline (Fig. 1C).

Next, we tested the efficacy of scavengers of various reactive species. To interfere intracellular redox homoeostasis, Tempol (a superoxide dismutase mimetic), PDTC (a NO synthase inhibitor) and NAC (preferentially reacting with reactive oxygen and nitrogen species) were used. Among these compounds only Tempol blunted DCF-fluorescence (Fig. 1D) and subsequent phosphorylation of p38 MAPK (Fig. 1E) in response to 15d-PGJ_2 treatment. These data reveal that the formation of reactive species is an upstream event of p38 MAPK activation.

3.3. Phosphorylation of AKT via p38 MAPK activation in response to 15d-PGJ_2

Fig. 2 shows that 15d-PGJ_2 treatment resulted in transient phosphorylation of Akt (T^{308}) reaching a plateau from 2 h (Fig. 2A). Pretreatment of cells with PD169316 (a p38 MAPK

inhibitor), LY294002 (an inhibitor of PI3K/Akt) as well as Akt-I (an Akt inhibitor) prevented Akt phosphorylation (Fig. 2B). These results indicate that 15d-PGJ_2-induced phosphorylation of Akt depends on the activation of p38 MAPK and PI3K.

3.4. Activation of Egr1 and Nrf2 via p38 MAPK/Akt signalling in response to 15d-PGJ_2

Next, we tested whether 15d-PGJ_2 promotes induction of transcriptional factors via the PI3K/Akt pathway. Indeed, 15d-PGJ_2 treatment resulted in a transient increase of both Nrf2 (2 h) and Egr1 (1 h) expression at mRNA level (Fig. 3A/B; upper panel). This was accompanied by an increase of Nrf2 and Egr1 protein, which lagged approximately 2 h behind mRNA levels (Fig. 3A/B; middle and lower panels). Western blot analysis of Nrf2 and Egr1 showed only faint cytosolic expression but intense signals in the nuclear fraction after 1 h (Nrf2) or 2 h (Egr1) in response to 15d-PGJ_2 (Fig. 3C, left and right panels, respectively). Pretreatment of MG-63 cells with LY294002 and Akt-I prevented induction of Nrf2 and Egr1 (Fig. 3D). These results demonstrate that 15d-PGJ_2-induced expression of Nrf2/Egr1 is mediated via the p38 MAPK/PI3K/Akt axis.

3.5. Activation of HO-1 and GCLc in response to 15d-PGJ_2

The 5′-untranslated region of *HMOX1* (the gene encoding human HO-1) contains antioxidant-response elements (AREs) that can bind the transcription factor Nrf2. Thereby Nrf2 elevates oxidative-stress-induced transcription of HO-1. Fig. 4A shows a time-dependent increase of HO-1 transcription (upper panel) and translation (middle and lower panels) in response to 15d-PGJ_2. Incubation of MG-63 cells with LY294002 or Akt-I prior to 15d-PGJ_2 treatment significantly impaired HO-1 expression (Fig. 4B). Silencing of Nrf2 or Egr1 with specific siRNAs significantly decreased immunoreactive HO-1 bands to almost baseline levels (Fig. 4C/D).

The protective gene *GCL* is under control of the transcriptional ARE of Nrf2 [36]. 15d-PGJ_2 treatment resulted in a time-dependent increase of GCLc on mRNA (Fig. 5A, upper panel) and protein levels (Fig. 5A, middle and lower panels), while expression of GCLm (the modifier subunit of GCL) was unaffected by 15d-PGJ_2 treatment (Fig. 5B). To demonstrate catalytic activity of GCLc intracellular GSH levels were quantitated by the Glutathione Assay kit. Time-course experiments show an increase of GSH levels reaching a plateau from 12 h (Fig. 5C). Preincubation of cells with LY294002 and Akt-I prior to 15d-PGJ_2 treatment blunted GCLc expression (Fig. 4B). Most importantly, silencing of Nrf2 or Egr1 decreased immunoreactive GCLc bands almost to baseline levels (Fig. 4C/D).

Next, we aimed to elucidate whether 15d-PGJ_2-mediated signalling occurs via receptor-dependent or -independent interaction. 15d-PGJ_2 is considered as a potent endogenous ligand for PPARγ, a member of the nuclear receptor superfamily of ligand-dependent transcriptional factors. T0070907 (a PPARγ antagonist) was unable to inhibit 15d-PGJ_2-induced HO-1 and GCLc expression (Fig. 5D). Then, we tested a possible involvement of PGD_2 receptors DP1 and DP2 (the latter also named CRTH2, the chemoattractant receptor-homologous molecule expressed on Th2 cells), which are reported to interact with 15d-PGJ_2 [18,37]. Of note, neither MK0524 (a DP1 antagonist) nor CAY10471 (a DP2 antagonist) altered expression levels of HO-1 and GCLc proteins in response to 15d-PGJ_2 (Fig. 5D).

3.6. 15d-PGJ_2 impairs metabolic activity and promotes cell death

Next, the MTT assay was performed to assess cell metabolic activity [38]. This colorimetric assay revealed a decrease of metabolic activity of MG-63 cells by 60% (24 h) and 80% (48 h) after 15d-PGJ_2 treatment (Fig. 6A), data in line with previous findings [30].

We tested whether these alterations are paralleled by induction of apoptosis. Pronounced immunoreactive bands of the respective cleavage product, caspase-3 (17 and 19 kDa) became apparent after 24 h (Fig. 6B). Activation of caspase-3 (the convergence point of the extrinsic and intrinsic apoptotic pathway) is the prerequisite for apoptotic cell death. Fig. 6B shows that 15d-PGJ_2 also promoted PARP cleavage (89 kDa), a downstream event of pro-caspase-3 cleavage.

To confirm that MG-63 cells undergo apoptosis, flow cytometry analyses using Annexin V/PI staining were performed. Fig. 7A shows representative scatter plots of MG-63 cells treated with 15d-PGJ_2 up to 48 h; staurosporine was used as a positive control to induce apoptosis. Fig. 7B summarizes the percentage of living, early/late apoptotic and necrotic cells. In vehicle-treatment group the number of early and late apoptotic cells was 11% and 3%, respectively. Time-dependent treatment with 15d-PGJ_2 significantly increased the percentage of early and late apoptotic cells up to 20% and 11%, respectively, after 48 h. The time-dependent decrease of living MG-63 cells (Fig. 7B) coincides with decreased MTT reduction (Fig. 6A) and activation of pro-caspase-3 and PARP (Fig. 6B).

3.7. The Nrf2/Egr1-HO-1/GCLc axis is a cell survival pathway protecting against 15d-PGJ_2-induced apoptosis

Next, we addressed possible survival pathways against 15d-PGJ_2-induced cell death in MG-63 cells. Performing the MTT assay we show that silencing of transcriptional factors Nrf2 and Egr1, as well as their downstream target, HO-1, with the specific siRNAs decreased cellular metabolic activity of 15d-PGJ_2-treated cells (Fig. 8A). Western blot experiments confirm that silencing of HO-1 increases cleavage of pro-caspase-3 and PARP in response to 15d-PGJ_2 (Fig. 8B).

Alternatively, MG-63 cells were treated with BSO (a specific inhibitor of GCL [39]) prior to 15d-PGJ_2 treatment. Similar to the silencing approach, BSO-pretreatment decreased cellular metabolic activity (Fig. 8A). In line, Western blot experiments reveal a more pronounced cleavage of pro-caspase-3 and PARP when compared to cells treated with 15d-PGJ_2 alone (Fig. 8C).

Next, MG-63 cells were preincubated with GSH ethyl ester to increase intracellular GSH levels. Indeed, GSH pretreatment protected MG-63 cells against 15d-PGJ_2-induced depletion of metabolic activity (Fig. 8A) and cleavage of pro-caspase-3 and PARP (Fig. 8D).

We were further interested whether interference with the intracellular redox balance would affect cell survival pathways. Fig. 9A (upper panel) shows that DCF fluorescence was reduced to baseline levels when cells were preincubated with GSH ethyl ester. In parallel, expression of Nrf2/Egr1 and HO-1/GCLc was significantly reduced in response to GSH ethyl ester (Fig. 9A; middle and lower panels). As an alternative approach, MG-63 cells

were pretreated with MPG, a precursor for intracellular GSH synthesis. MPG decreased DCF-fluorescence (Fig. 9A; upper panel) and protein expression of Nrf2/Egr1 and HO-1/GCLc (Fig. 9A; middle and lower panels) in response to 15d-PGJ_2.

Finally, data in Fig. 9B show that pretreatment of MG-63 cells with 5 mM MPG blunted 15d-PGJ_2-induced cleavage of pro-caspase 3 and PARP.

3.8. Effects of dh-15d-PGJ_2, the structural analogue of 15d-PGJ_2

To prove that the C9 electrophilic carbon atom of 15d-PGJ_2 (for structure, see Fig. 10A, [16]) is a prerequisite for 15d-PGJ_2-mediated signalling, we included dh-15d-PGJ_2, a structural analogue of 15d-PGJ_2 lacking the α,β-unsaturated ketone structural element (Fig. 10A) [18,30]. We have previously shown in MG-63 cells that dh-15d-PGJ_2 did not induce ROS formation, an apparent prerequisite for MAPK activation [30]. Here, we show that in contrast to 15d-PGJ_2, dh-15d-PGJ_2 did neither induce phosphorylation of p38 MAPK/Akt, expression of Nrf2/Egr1 and HO-1/GCLc nor cleavage of pro-caspase-3/PARP in MG-63 cells (Fig. 10B–F).

4. Discussion

Increased production of ROS is the characteristic of a metabolic shift observed during malignant transformation. Therefore, maintaining redox balance is crucial for cancer cell survival and might be exploited pharmacologically [29,40]. However, redox alteration in cancer cells is complex and addition of ROS-generating agents may not always lead to preferential cell killing. Cancer cells may become well adapted to stress and may develop a selective, endogenous antioxidant defence system to promote cell proliferation and evade apoptosis [29,40,41]. Therefore, we were interested if such a mechanism operates in OS and whether modulation of these pathways elevates apoptosis.

Here, we present evidence for the induction of the Nrf2-Egr1/HO-1-GCLc signalling pathway in response to 15d-PGJ_2 in MG-63 cells. Genetic or pharmacological interference at specific steps of this pathway modulated cell metabolic activity and cleavage of pro-caspase-3 and PARP (a hallmark of apoptosis). To the best of our knowledge we are the first to show that activation of the MAPK/Akt/Nrf2-Egr1/HO-1-GCLc axis provides an adaptive survival response of MG-63 OS cells against 15d-PGJ_2-induced treatment (Fig. 11). Most importantly, the observed effects are independent of PPARγ and PGD_2 receptors, DP1 and DP2.

The lipocalin-type PGD_2 synthase is abundantly expressed in primary osteoblasts and MG-63 cells [6,42] and both cells synthesize PGD_2 in vitro in response to various stimuli [6]. As an autacoid, PGD_2 can act on DP1 and DP2 receptors, both present on osteoblasts and MG-63 [6] as well osteoclasts [43]. In the latter cell type PGD_2-induced apoptosis was exclusively mediated by the DP2-p42/44 MAPK-Akt axis without involvement of DP1 [5,44]. However, PGD_2 is rapidly metabolized into PGs of the J-series; therefore it is reasonable to assume that 15d-PGJ_2 is most likely responsible for the effects observed with its parent PG. While a series of reports addressed PPARγ-independent activities of 15d-PGJ_2, less information is available on DP1- and/or DP2-receptor-mediated downstream

cellular signalling and apoptosis. In cardiomyocytes 15d-PGJ_2 promoted inflammation and apoptosis via the DP2/MAPK/TNF α axis [18], while in murine oligodendrocytes [45] and human MG-63 cells (Fig. 5B) neither DP1 nor DP2 receptor was involved.

15d-PGJ_2 is highly reactive [16,17] and rapidly gets inactivated by the components of cell culture medium, and therefore the concentrations of 15d-PGJ_2 used under in vitro conditions are much higher than those of estimated under in vivo conditions [37]. Furthermore, estimated in vivo levels of 15d-PGJ_2 represent only the freely available (but not protein-/thiol-inactivated) eicosanoid. Therefore, we have used a concentration of 20 μM 15d-PGJ_2 as a bolus in the present vitro study. Moreover, it is worth mentioning that primary cells are much more sensitive to 15d-PGJ_2 treatment compared to immortalized cell lines [18].

In line with our previous data, we show that 15d-PGJ_2 rapidly initiates phosphorylation of p38 MAPK in MG-63 cells (Fig. 1A/B) while pronounced activation of p42/44 MAPK occurred from 4 h [30]. In addition, we show that altered redox homoeostasis is the trigger for p38 MAPK activation (Fig. 1C/D), which in turn promoted Akt phosphorylation (Fig. 2). Indeed, the PI3K/Akt pathway is considered as one of the most important pro-survival pathways in human OS (for a review see [46]). Since Akt promotes survival of cancer cells even under adverse conditions and during chemotherapy, hyperactivated Akt in OS represents the platform for disease initiation and propagation. Activation of the PI3K/Akt axis in cancer cells promotes cell cycle progression, invasion, proliferation, angiogenesis, tumourigenesis and metastasis but inhibits apoptosis. Therefore, modulation of the PI3/Akt axis could represent a therapeutic option [46]. Results of the present study demonstrate that LY294002 (PI3K/Akt) and Akt-I effectively blocked survival signalling in MG-63 cells via the ARE pathway (Figs. 2 and 4). Previously, inhibition of Akt by natural compounds e.g. Grifolin and Oridonin has been reported to induce caspase-dependent apoptosis in OS cells [47,48]. Moreover, Miwa and colleagues [49] reported that caffeine induces apoptosis in OS cells via activation of PTEN (phosphatase and tensin homologue), a negative regulator of PI3K-Akt signalling.

Following endogenous or exogenous oxidative stress response, sequential activation of MAPK and Akt induces expression of Egr1 and Nrf2. While expression of Egr1 and downstream targets is linked to cell cycle regulation, growth, proliferation and migration, an active Nrf2 pathway maintains redox balance in cancer cells in a range that favours cell growth and survival [50]. Thus, Nrf2 and its downstream target(s) including HO-1 appear to induce chemoresistance in cancer cells. In contrast, Egr1 regulates HO-1 expression in various cells/tissues [51,52] but no report is available for OS cells. Under unstressed conditions, expression of HO-1 in osteoblasts is very low [53]. In line, our results show almost no detectable HO-1 protein in OS cells under non-stimulated conditions (Fig. 4A). However, overexpression of HO-1 may increase osteoblast differentiation [54]. Most importantly, HO-1 upregulation protects mesenchymal stem cells [55] and cancer cells [56] against chemotherapeutic compounds. Inhibition of HO-1 increases responsiveness of pancreatic cancer cells against chemotherapy [57] and elevates apoptosis-induced cell death in MG-63 cells (Fig. 7B). Indeed, silencing of Nrf2, Egr1 and HO-1 (Fig. 8A) must be considered an effective approach to impair survival signalling of MG-63 OS cells.

The GSH redox and detoxification system is a critical cellular homoeostatic mechanism [58]. When cancer cells internalize anti-neoplastic drugs they might be conjugated with GSH and metabolized. Thus elevated GSH levels or increased activity of GCLc as observed here can decrease drug efficacy. The first and rate-limiting step in GSH synthesis is catalysed by GCL, a heterodimeric protein composed of GCLc and GCLm subunits both expressed by separate genes. GCLc exhibits all of the catalytic activity while GCLm is inactive but regulates the reaction rate and catalytic activity of GCLc to produce GSH [59]. Transcription of GCLc and GCLm is under control of the ARE pathway and expression of Nrf2 and GCLc in sarcoma tissues suggests that this protective pathway might be active in most sarcomas [60]. While only little information is available about interaction of Egr1 with GCLc promoter [61], our data confirm the regulation of GCLc expression via transcriptional factor Egr1 in MG-63 OS cells (Fig. 4D). In the pheochromocytoma PC12 cell line both GCL subunits were upregulated in response to 15d-PGJ_2 [62]. In contrast, oxidative stress conditions appear to induce selectively the transcription of GCLc subunit in human hepatocellular carcinoma [62]. These data are in line with our findings where 15d-PGJ_2 specifically increases GCLc protein and intracellular GSH levels in MG-63 OS cells.

Because of the electrophilic α,β-unsaturated ketone moiety, 15d-PGJ_2 acts as an endogenous electrophile. 15d-PGJ_2 may form covalent protein adducts via Michael addition with cellular nucleophiles, such as thiol groups of proteins [63]. In comparison to other reactive aldehydes like 4-hydroxynonenal or acrolein, 15d-PGJ_2 is less reactive but displays higher target specificity [64]. This is of relevance for the present study, since 15d-PGJ_2 induces ARE via covalent thiol-modification in Keap1. Under basal conditions two molecules of Keap1 interact with one Nrf2 molecule where Keap1 functions as an adaptor protein in the Cullin3-based E3 ligase system that facilitates ubiquitination and proteasomal degradation of Nrf2 [65]. 15d-PGJ_2 modifications at thiol residues induce a conformational change in Keap1, displacement of the DLG motif, leading to the escape of Nrf2 from proteasomal degradation. In this electrophile-activated setting, Nrf2 translocates to the nucleus, binds to ARE (following dimerization with small Maf proteins) and induces downstream target gene transcription including HO-1, GCLm, and GCLc [65]. Our observation that dh-15d-PGJ_2 (lacking the endocyclic double bond) is unable to reproduce the biological activities of 15d-PGJ_2 (Fig. 10) supports the concept of covalent electrophile modification during ARE induction in MG-63 cells.

During the present study we chose two different experimental approaches to modulate intracellular GSH levels namely (i) to provide extracellular cell-permeable precursors (GSH ethyl ester and MPG) and (ii) to pharmacologically inhibit GCLc with BSO. Due to the ability of 15d-PGJ_2 to form covalent adducts with thiols (see above) we cannot exclude that some 15d-PGJ_2 is scavenged by GSH ethyl ester and/or MPG in the cellular supernatant thus reducing active 15d-PGJ_2. BSO, an inhibitor of cellular GSH synthesis, significantly augmented the apoptotic potential of 15d-PGJ_2 towards MG-63 cells. This is reminiscent of what was reported for andrographolide-treated hepatoma cells [66] or Cisplatin-treated OS cells [67].

Tumour suppressor *p53* is the most frequently mutated/deleted gene in OS [1,68]. Therefore, we have used MG-63 cells (that lack p53) as a suitable and representative OS cell model.

Our data reveal that ROS generated by 15d-PGJ_2 in MG-63 cells induces apoptosis in a p53-independent manner. Alternatively, retinoblastoma (Rb) protein (expressed in MG-63 [69]), that controls activation of the E2F transcription factor family, might be involved in the observed cell death signalling. In particular, E2F1 is known to induce apoptosis via p53-independent pathways and to regulate expression of various genes that play pivotal role in the apoptotic machinery and DNA damage [70]. Furthermore, Rb interacts with PTEN that modulates phosphorylation of Akt via PDK, an important cancer survival pathway including OS. Another mode of action could involve inhibition of anti-apoptotic activity of the transcriptional factor NF-κB by 15d-PGJ_2. In ovarian cancer cells 15d-PGJ_2 inhibited NF-κB activity in a concentration-dependent manner, whereby complete inhibition was observed at 20 μM [71], a concentration that was used also in the present study. As 15d-PGJ_2-induced ROS formation has been reported to inhibit NF-κB activity in endothelial cells [72], this pathway might be operative to induce 15d-PGJ_2-mediated apoptosis in MG-63 cells after 24 h.

In conclusion, our data provide a framework for the construction of cell death and cell survival pathways in MG-63 OS cells in response to 15d-PGJ_2 (Fig. 11). The survival pathway originates from p38 MAPK activation that extends to Akt-mediated translocation of Nrf2/Egr1 to the nucleus and upregulation of HO-1/GCLc expression. HO-1 and GSH protected cells against 15d-PGJ_2-induced pro-caspase-3 and PARP cleavage and cell death. Silencing of Nrf2, Egr1 and HO-1, and inhibition of GSH synthesis by BSO sensitized MG-63 cells towards 15d-PGJ_2-induced apoptosis.

Acknowledgments

C.K. was funded by the Austrian Science Fund (FWF, W1226-B18) within the “Doctoral College Metabolic and Cardiovascular Disease”. K.K. was funded by the Ph.D. Program “Molecular Medicine” at the Medical University of Graz. This work further received support from FWF, W1241 (“Doctoral College – MOLIN”). We thank L. Frank for technical assistance.

References

[1]. Kansara M, Teng MW, Smyth MJ, Thomas DM. Translational biology of osteosarcoma. Nat. Rev. Cancer. 2014; 14:722–735. [PubMed: 25319867]

[2]. Ottaviani G, Jaffe N. The etiology of osteosarcoma. Cancer Treat. Res. 2009; 152:15–32. [PubMed: 20213384]

[3]. Hikiji H, Takato T, Shimizu T, Ishii S. The roles of prostanoids, leukotrienes, and platelet-activating factor in bone metabolism and disease. Prog. Lipid Res. 2008; 47:107–126. [PubMed: 18187046]

[4]. During A, Penel G, Hardouin P. Understanding the local actions of lipids in bone physiology. Prog. Lipid Res. 2015; 59:126–146. [PubMed: 26118851]

[5]. Yue L, Durand M, Jacob M.C. Lebeau, Hogan P, McManus S, Roux S, et al. Prostaglandin D2 induces apoptosis of human osteoclasts by activating the CRTH2 receptor and the intrinsic apoptosis pathway. Bone. 2012; 51:338–346. [PubMed: 22705147]

[6]. Gallant MA, Samadfam R, Hackett JA, Antoniou J, Parent JL, de Brum-Fernandes AJ. Production of prostaglandin D(2) by human osteoblasts and modulation of osteoprotegerin, RANKL, and cellular migration by DP and CRTH2 receptors. J. Bone Miner. Res. 2005; 20:672–681. [PubMed: 15765187]

[7]. Koshihara Y, Kawamura M. Prostaglandin D2 stimulates calcification of human osteoblastic cells. Biochem. Biophys. Res. Commun. 1989; 159:1206–1212. [PubMed: 2930558]

[8]. Kuroyanagi G, Mizutani J, Kondo A, Yamamoto N, Matsushima-Nishiwaki R, Otsuka T, et al. Suppression by resveratrol of prostaglandin D2-stimulated osteoprotegerin synthesis in osteoblasts. Prostaglandins Leukot. Essent. Fatty Acids. 2014; 91:73–80. [PubMed: 24813642]

[9]. Tokuda H, Kozawa O, Harada A, Uematsu T. Prostaglandin D2 induces interleukin-6 synthesis via Ca^{2+} mobilization in osteoblasts: regulation by protein kinase C. Prostaglandins Leukot. Essent. Fatty Acids. 1999; 61:189–194. [PubMed: 10582659]

[10]. Tokuda H, Takai S, Matsushima-Nishiwaki R, Hanai Y, Adachi S, Minamitani C, et al. Function of rho-kinase in prostaglandin D2-induced interleukin-6 synthesis in osteoblasts. Prostaglandins Leukot. Essent. Fatty Acids. 2008; 79:41–46. [PubMed: 18771907]

[11]. Kozawa O, Otsuka T, Hatakeyama D, Niwa M, Matsuno H, Ito H, et al. Mechanism of prostaglandin D(2)-stimulated heat shock protein 27 induction in osteoblasts. Cell. Signal. 2001; 13:535–541. [PubMed: 11483406]

[12]. Kato K, Tokuda H, Natsume H, Adachi S, Matsushima-Nishiwaki R, Minamitani C, et al. Rho-kinase regulates prostaglandin D(2)-stimulated heat shock protein 27 induction in osteoblasts. Exp. Ther. Med. 2010; 1:579–583. [PubMed: 22993579]

[13]. Schuligoi R, Schmidt R, Geisslinger G, Kollroser M, Peskar BA, Heinemann A. PGD2 metabolism in plasma: kinetics and relationship with bioactivity on DP1 and CRTH2 receptors. Biochem. Pharmacol. 2007; 74:107–117. [PubMed: 17452035]

[14]. Powell WS. 15-Deoxy-delta12,14-PGJ2: endogenous PPARgamma ligand or minor eicosanoid degradation product? J Clin. Invest. 2003; 112:828–830. [PubMed: 12975467]

[15]. Shibata T, Kondo M, Osawa T, Shibata N, Kobayashi M, Uchida K. 15-Deoxy-delta 12,14-prostaglandin J2. A prostaglandin D2 metabolite generated during inflammatory processes. J. Biol. Chem. 2002; 277:10459–10466. [PubMed: 11786541]

[16]. Uchida K, Shibata T. 15-Deoxy-Delta(12,14)-prostaglandin J2: an electrophilic trigger of cellular responses. Chem. Res. Toxicol. 2008; 21:138–144. [PubMed: 18052108]

[17]. Straus DS, Glass CK. Cyclopentenone prostaglandins: new insights on biological activities and cellular targets. Med. Res. Rev. 2001; 21:185–210. [PubMed: 11301410]

[18]. Koyani CN, Windischhofer W, Rossmann C, Jin G, Kickmaier S, Heinzel FR, et al. 15-Deoxy-Delta(1)(2), (1)(4)-PGJ(2) promotes inflammation and apoptosis in cardiomyocytes via the DP2/MAPK/TNFalpha axis. Int. J. Cardiol. 2014; 173:472–480. [PubMed: 24698234]

[19]. Bishop-Bailey D, Hla T. Endothelial cell apoptosis induced by the peroxisome proliferator-activated receptor (PPAR) ligand 15-deoxy-Delta 12, 14-prostaglandin J2. J. Biol. Chem. 1999; 274:17042–17048. [PubMed: 10358055]

[20]. Kawahito Y, Kondo M, Tsubouchi Y, Hashiramoto A, Bishop-Bailey D, Inoue K, et al. 15-Deoxy-delta(12,14)-PGJ(2) induces synoviocyte apoptosis and suppresses adjuvant-induced arthritis in rats. J. Clin. Invest. 2000; 106:189–197. [PubMed: 10903334]

[21]. Ray DM, Akbiyik F, Phipps RP. The peroxisome proliferator-activated receptor gamma (PPARgamma) ligands 15-deoxy-Delta 12,14-prostaglandin J2 and ciglitazone induce human B lymphocyte and B cell lymphoma apoptosis by PPARgamma-independent mechanisms. J. Immunol. 2006; 177:5068–5076. [PubMed: 17015690]

[22]. Levonen AL, Dickinson DA, Moellering DR, Mulcahy RT, Forman HJ, Darley-Usmar VM. Biphasic effects of 15-deoxy-delta(12,14)-prostaglandin J(2) on glutathione induction and apoptosis in human endothelial cells. Arterioscler. Thromb. Vasc. Biol. 2001; 21:1846–1851. [PubMed: 11701476]

[23]. Sakaba Y, Awata H, Morisugi T, Kawakami T, Sakudo A, Tanaka Y. 15-Deoxy-Delta 12,14-prostaglandin J2 induces PPARgamma- and p53-independent apoptosis in rabbit synovial cells. Prostaglandins Other Lipid Mediat. 2014; 109–111:1–13.

[24]. Li L, Tao J, Davaille J, Feral C, Mallat A, Rieusset J, et al. 15-Deoxy-Delta 12,14-prostaglandin J2 induces apoptosis of human hepatic myofibroblasts. A pathway involving oxidative stress independently of peroxisome-proliferator-activated receptors. J. Biol. Chem. 2001; 276:38152–38158. [PubMed: 11477100]

[25]. Okano H, Shiraki K, Inoue H, Yamanaka Y, Kawakita T, Saitou Y, et al. 15-Deoxy-delta-12-14-PGJ2 regulates apoptosis induction and nuclear factor-kappaB activation via a peroxisome

Europe PMC Funders Author Manuscripts

proliferator-activated receptor-gamma-independent mechanism in hepatocellular carcinoma. Lab. Invest. 2003; 83:1529–1539. [PubMed: 14563954]

[26]. Napimoga MH, Demasi AP, Bossonaro JP, de Araujo VC, Clemente-Napimoga JT, Martinez EF. Low doses of 15d-PGJ2 induce osteoblast activity in a PPAR-gamma independent manner. Int. Immunopharmacol. 2013; 16:131–138. [PubMed: 23597428]

[27]. Lee SJ, Kim MS, Park JY, Woo JS, Kim YK. 15-Deoxy-delta 12,14-prostaglandin J2 induces apoptosis via JNK-mediated mitochondrial pathway in osteoblastic cells. Toxicology. 2008; 248:121–129. [PubMed: 18450357]

[28]. Yen CC, Hsiao CD, Chen WM, Wen YS, Lin YC, Chang TW, et al. Cytotoxic effects of 15d-PGJ2 against osteosarcoma through ROS-mediated AKT and cell cycle inhibition. Oncotarget. 2014; 5:716–725. [PubMed: 24566468]

[29]. Trachootham D, Alexandre J, Huang P. Targeting cancer cells by ROS-mediated mechanisms: a radical therapeutic approach? Nat Rev. Drug Discov. 2009; 8:579–591. [PubMed: 19478820]

[30]. Kitz K, Windischhofer W, Leis HJ, Huber E, Kollroser M, Malle E. 15-Deoxy-Delta 12,14-prostaglandin J2 induces Cox-2 expression in human osteosarcoma cells through MAPK and EGFR activation involving reactive oxygen species. Free Radic. Biol. Med. 2011; 50:854–865. [PubMed: 21236332]

[31]. Windischhofer W, Huber E, Rossmann C, Semlitsch M, Kitz K, Rauh A, et al. LPA-induced suppression of periostin in human osteosarcoma cells is mediated by the LPA(1)/Egr-1 axis. Biochimie. 2012; 94:1997–2005. [PubMed: 22659570]

[32]. Rauh A, Windischhofer W, Kovacevic A, DeVaney T, Huber E, Semlitsch M, et al. Endothelin (ET)-1 and ET-3 promote expression of c-fos and c-jun in human choriocarcinoma via ET(B) receptor-mediated G(i)- and G(q)-pathways and MAP kinase activation. Br. J. Pharmacol. 2008; 154:13–24. [PubMed: 18362896]

[33]. Bernhart E, Damm S, Wintersperger A, Nusshold C, Brunner AM, Plastira I, et al. Interference with distinct steps of sphingolipid synthesis and signaling attenuates proliferation of U87MG glioma cells. Biochem. Pharmacol. 2015; 96:119–130. [PubMed: 26002572]

[34]. Semlitsch M, Shackelford RE, Zirkl S, Sattler W, Malle E. ATM protects against oxidative stress induced by oxidized low-density lipoprotein. DNA Repair. 2011; 10:848–860. [PubMed: 21669554]

[35]. Lin TH, Tang CH, Hung SY, Liu SH, Lin YM, Fu WM, et al. Upregulation of heme oxygenase-1 inhibits the maturation and mineralization of osteoblasts. J. Cell. Physiol. 2010; 222:757–768. [PubMed: 20020468]

[36]. Yang H, Magilnick N, Lee C, Kalmaz D, Ou X, Chan JY, et al. Nrf1 and Nrf2 regulate rat glutamate-cysteine ligase catalytic subunit transcription indirectly via NF-kappaB and AP-1. Mol. Cell. Biol. 2005; 25:5933–5946. [PubMed: 15988009]

[37]. Rajakariar R, Hilliard M, Lawrence T, Trivedi S, Colville-Nash P, Bellingan G, et al. Hematopoietic prostaglandin D2 synthase controls the onset and resolution of acute inflammation through PGD2 and 15-deoxyDelta12 14 PGJ2. Proc. Natl. Acad. Sci. U.S.A. 2007; 104:20979–20984. [PubMed: 18077391]

[38]. Berridge MV, Herst PM, Tan AS. Tetrazolium dyes as tools in cell biology: new insights into their cellular reduction. Biotechnol. Annu. Rev. 2005; 11:127–152. [PubMed: 16216776]

[39]. Drew R, Miners JO. The effects of buthionine sulphoximine (BSO) on glutathione depletion and xenobiotic biotransformation. Biochem. Pharmacol. 1984; 33:2989–2994. [PubMed: 6148944]

[40]. Acharya A, Das I, Chandhok D, Saha T. Redox regulation in cancer: a double-edged sword with therapeutic potential. Oxid. Med. Cell. Longevity. 2010; 3:23–34.

[41]. Liou GY, Storz P. Reactive oxygen species in cancer. Free Radic. Res. 2010; 44:479–496. [PubMed: 20370557]

[42]. Mathurin K, Gallant MA, Germain P, Allard-Chamard H, Brisson J, Iorio-Morin C, et al. An interaction between L-prostaglandin D synthase and arrestin increases PGD2 production. J. Biol. Chem. 2011; 286:2696–2706. [PubMed: 21112970]

[43]. Durand M, Gallant MA, de Brum-Fernandes AJ. Prostaglandin D2 receptors control osteoclastogenesis and the activity of human osteoclasts. J. Bone Miner. Res. 2008; 23:1097–1105. [PubMed: 18302497]

[44]. Yue L, Haroun S, Parent JL, de Brum-Fernandes AJ. Prostaglandin D(2) induces apoptosis of human osteoclasts through ERK1/2 and Akt signaling pathways. Bone. 2014; 60:112–121. [PubMed: 24345643]

[45]. Xiang Z, Lin T, Reeves SA. 15d-PGJ2 induces apoptosis of mouse oligodendrocyte precursor cells. J. Neuroinflamm. 2007; 4:18.

[46]. Zhang J, Yu XH, Yan YG, Wang C, Wang WJ. PI3K/Akt signaling in osteosarcoma. Clin. Chim. Acta. 2015; 444:182–192. [PubMed: 25704303]

[47]. Jin S, Pang RP, Shen JN, Huang G, Wang J, Zhou JG. Grifolin induces apoptosis via inhibition of PI3K/AKT signalling pathway in human osteosarcoma cells. Apoptosis. 2007; 12:1317–1326. [PubMed: 17333316]

[48]. Jin S, Shen JN, Wang J, Huang G, Zhou JG. Oridonin induced apoptosis through Akt and MAPKs signaling pathways in human osteosarcoma cells. Cancer Biol. Ther. 2007; 6:261–268. [PubMed: 17218775]

[49]. Miwa S, Sugimoto N, Shirai T, Hayashi K, Nishida H, Ohnari I, et al. Caffeine activates tumor suppressor PTEN in sarcoma cells. Int. J. Oncol. 2011; 39:465–472. [PubMed: 21617855]

[50]. Na HK, Surh YJ. Oncogenic potential of Nrf2 and its principal target protein heme oxygenase-1. Free Radic. Biol. Med. 2014; 67:353–365. [PubMed: 24200599]

[51]. Chen H, Wang L, Gong T, Yu Y, Zhu C, Li F, et al. EGR-1 regulates Ho-1 expression induced by cigarette smoke. Biochem. Biophys. Res. Commun. 2010; 396:388–393. [PubMed: 20417178]

[52]. Wu H, Lei S, Yuan J, Liu X, Zhang D, Gu X, et al. Ischemic postconditioning downregulates Egr-1 expression and attenuates postischemic pulmonary inflammatory cytokine release and tissue injury in rats. J. Surg. Res. 2013; 181:204–212. [PubMed: 22878149]

[53]. Rawlinson SC, Zaman G, Mosley JR, Pitsillides AA, Lanyon LE. Heme oxygenase isozymes in bone: induction of HO-1 mRNA following physiological levels of mechanical loading in vivo. Bone. 1998; 23:433–436. [PubMed: 9823449]

[54]. Barbagallo I, Vanella A, Peterson SJ, Kim DH, Tibullo D, Giallongo C, et al. Overexpression of heme oxygenase-1 increases human osteoblast stem cell differentiation. J. Bone Miner. Metab. 2010; 28:276–288. [PubMed: 19924377]

[55]. Chen S, Wang J, Fang Q, Gao R, Shi Q, Zhang H, et al. Upregulated heme oxygenase-1 expression of mouse mesenchymal stem cells resists to chemotherapy-induced bone marrow suppression. Chin. Med. J. (Engl.). 2014; 127:1310–1316. [PubMed: 24709186]

[56]. Kongpetch S, Kukongviriyapan V, Prawan A, Senggunprai L, Kukongviriyapan U, Buranrat B. Crucial role of heme oxygenase-1 on the sensitivity of cholangiocarcinoma cells to chemotherapeutic agents. PLoS One. 2012; 7:e34994. [PubMed: 22514698]

[57]. Berberat PO, Dambrauskas Z, Gulbinas A, Giese T, Giese N, Kunzli B, et al. Inhibition of heme oxygenase-1 increases responsiveness of pancreatic cancer cells to anticancer treatment. Clin. Cancer Res. 2005; 11:3790–3798. [PubMed: 15897578]

[58]. Zhang H, Forman HJ. Glutathione synthesis and its role in redox signaling. Semin. Cell Dev. Biol. 2012; 23:722–728. [PubMed: 22504020]

[59]. Lu SC. Glutathione synthesis. Biochim. Biophys. Acta. 2013; 1830:3143–3153. [PubMed: 22995213]

[60]. Je EM, An CH, Yoo NJ, Lee SH. Mutational and expressional analyses of NRF2 and KEAP1 in sarcomas. Tumori. 2012; 98:510–515. [PubMed: 23052169]

[61]. Chang SY, Cho JM, Kim DB, Jang HJ, Ko SH, Jo YH, et al. Molecular mechanisms of early growth response protein-1 (EGR-1) expression by quercetin in INS-1 beta-cells. J. Cell. Biochem. 2012; 113:1559–1568. [PubMed: 22174042]

[62]. Chen ZH, Yoshida Y, Saito Y, Sekine A, Noguchi N, Niki E. Induction of adaptive response and enhancement of PC12 cell tolerance by 7-hydroxycholesterol and 15-deoxy-delta(12,14)-prostaglandin J2 through up-regulation of cellular glutathione via different mechanisms. J. Biol. Chem. 2006; 281:14440–14445. [PubMed: 16565077]

[63]. Shibata T. 15-Deoxy-Delta(1)(2), (1)(4)-prostaglandin J(2) as an electrophilic mediator. Biosci. Biotechnol. Biochem. 2015; 79:1044–1049. [PubMed: 26011133]

[64]. Wall SB, Oh JY, Diers AR, Landar A. Oxidative modification of proteins: an emerging mechanism of cell signaling. Front. Physiol. 2012; 3:369. [PubMed: 23049513]

[65]. Kansanen E, Kivela AM, Levonen AL. Regulation of Nrf2-dependent gene expression by 15-deoxy-Delta 12,14-prostaglandin J2. Free Radic. Biol. Med. 2009; 47:1310–1317. [PubMed: 19573595]

[66]. Ji L, Shen K, Jiang P, Morahan G, Wang Z. Critical roles of cellular glutathione homeostasis and jnk activation in andrographolide-mediated apoptotic cell death in human hepatoma cells. Mol. Carcinog. 2011; 50:580–591. [PubMed: 21319226]

[67]. Komiya S, Gebhardt MC, Mangham DC, Inoue A. Role of glutathione in cisplatin resistance in osteosarcoma cell lines. J. Orthop. Res. 1998; 16:15–22. [PubMed: 9565068]

[68]. Chen X, Bahrami A, Pappo A, Easton J, Dalton J, Hedlund E, et al. Recurrent somatic structural variations contribute to tumorigenesis in pediatric osteosarcoma. Cell Rep. 2014; 7:104–112. [PubMed: 24703847]

[69]. Hellwinkel OJ, Muller J, Pollmann A, Kabisch H. Osteosarcoma cell lines display variable individual reactions on wildtype p53 and Rb tumour-suppressor transgenes. J. Gene Med. 2005; 7:407–419. [PubMed: 15538723]

[70]. Ginsberg D. E2F1 pathways to apoptosis. FEBS Lett. 2002; 529:122–125. [PubMed: 12354623]

[71]. de Jong E, Winkel P, Poelstra K, Prakash J. Anticancer effects of 15dprostaglandin-J2 in wild-type and doxorubicin-resistant ovarian cancer cells: novel actions on SIRT1 and HDAC. PLoS One. 2011; 6:e25192. [PubMed: 21957481]

[72]. Ho TC, Chen SL, Yang YC, Chen CY, Feng FP, Hsieh JW, et al. 15-Deoxy-Delta(12,14)-prostaglandin J2 induces vascular endothelial cell apoptosis through the sequential activation of MAPKS and p53. J. Biol. Chem. 2008; 283:30273–30288. [PubMed: 18718914]

Europe PMC Funders Author Manuscripts

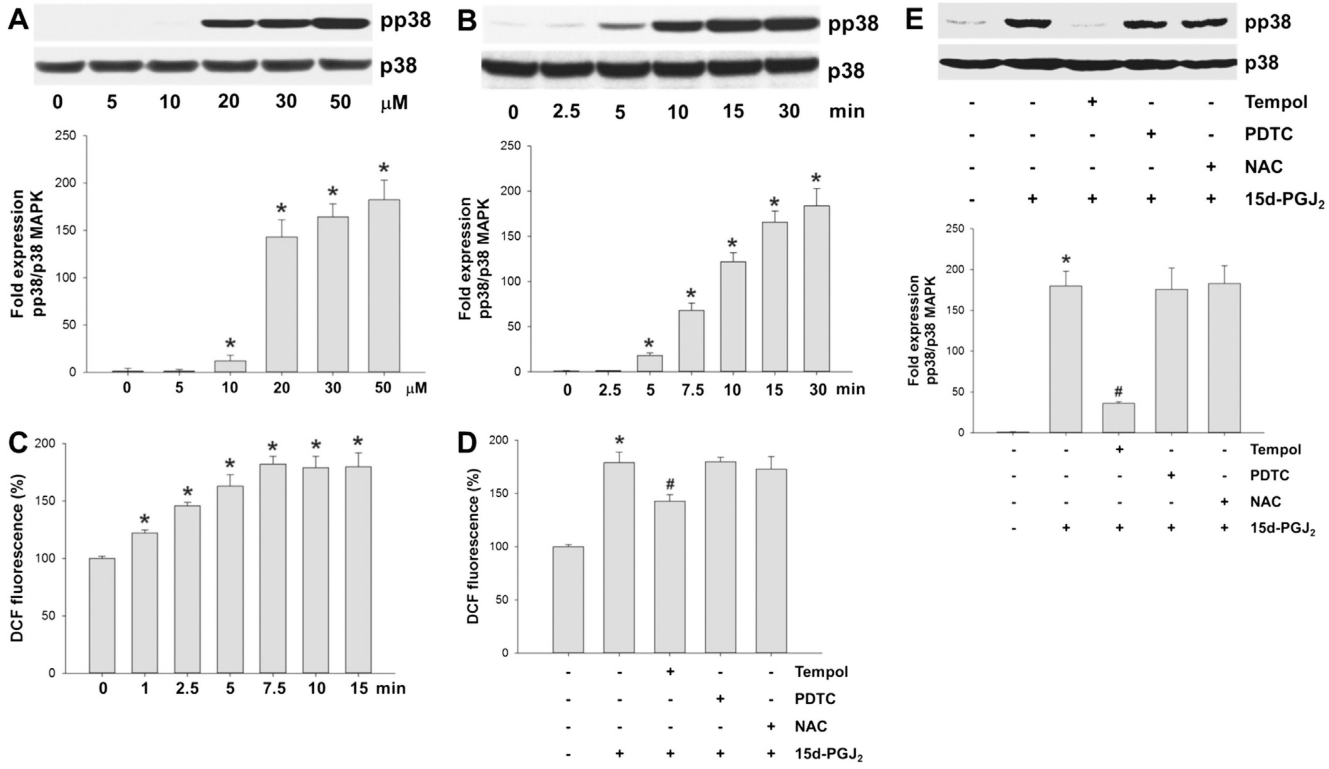

Fig. 1.

Activation of p38 MAPK via intracellular redox imbalance in response to 15d-PGJ_2. (A) MG-63 cells were treated with indicated concentrations of 15d-PGJ_2 for 10 min to follow pp38 MAPK expression using Western blot analysis. Cells were incubated with 15d-PGJ_2 (20 μM) for indicated time periods to follow (B) p38 MAPK activation (Western blot analysis) and (C) DCF fluorescence as an indicator of the intracellular redox balance. Cells were incubated with Tempol [1 mM], NAC [5 mM] or PDTC [1 mM] for 30 min prior to 15d-PGJ_2 treatment (20 μM) for 15 min to follow (D) ROS generation and (E) pp38 MAPK expression. Total p38 MAPK expression was used as a loading control. One representative blot (A/B/E [upper panel]) out of three is shown. Densitometric evaluation of immunoreactive bands is given below (A/B/E [lower panel]). Values are expressed as mean ± SEM ($n = 3$). For detection of intracellular ROS levels cells were incubated with carboxy-H_2DCFDA (10 μM) for 30 min after treatment with 15d-PGJ_2. DCF fluorescence intensity of vehicle (0.1% DMSO)-treated cells was set 100% and values are expressed as mean ± SEM ($n = 6$, C/D). $^{*}p \leqslant 0.05$ vs. control; $^{\#}p \leqslant 0.05$ vs. 15d-PGJ_2.

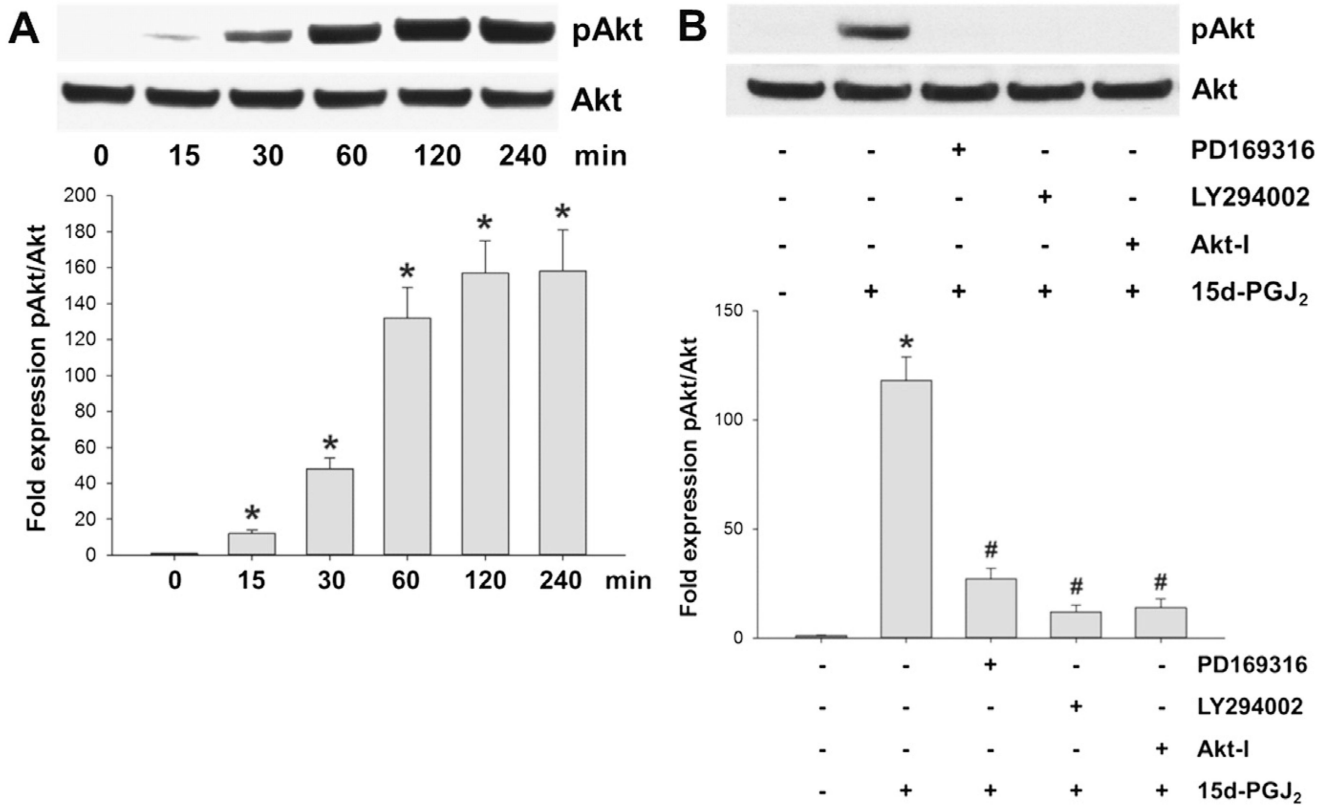

Fig. 2.

15d-PGJ_2 promotes Akt phosphorylation via p38 MAPK activation. (A) MG-63 cells were treated with 15d-PGJ_2 (20 μM) for indicated time periods to follow Akt phosphorylation (pAkt, T^{308}) using Western blot analysis. (B) Cells were incubated with PD169316 (25 μM), LY294002 (10 μM) or Akt-I (5 μM) for 30 min prior to 15d-PGJ_2 treatment (20 μM) for 1 h to follow pAkt expression. For Western blot analysis total protein lysates were subjected to SDS–PAGE. Total Akt expression was used as loading control. One representative blot (A/B [upper panel]) out of three is shown. Densitometric evaluation of immunoreactive bands is given below (A/B [lower panel]). Values are expressed as mean ± SEM ($n = 3$). $^{*}p \leqslant 0.05$ vs. control; $^{\#}p \leqslant 0.05$ vs. 15d-PGJ_2.

Europe PMC Funders Author Manuscripts

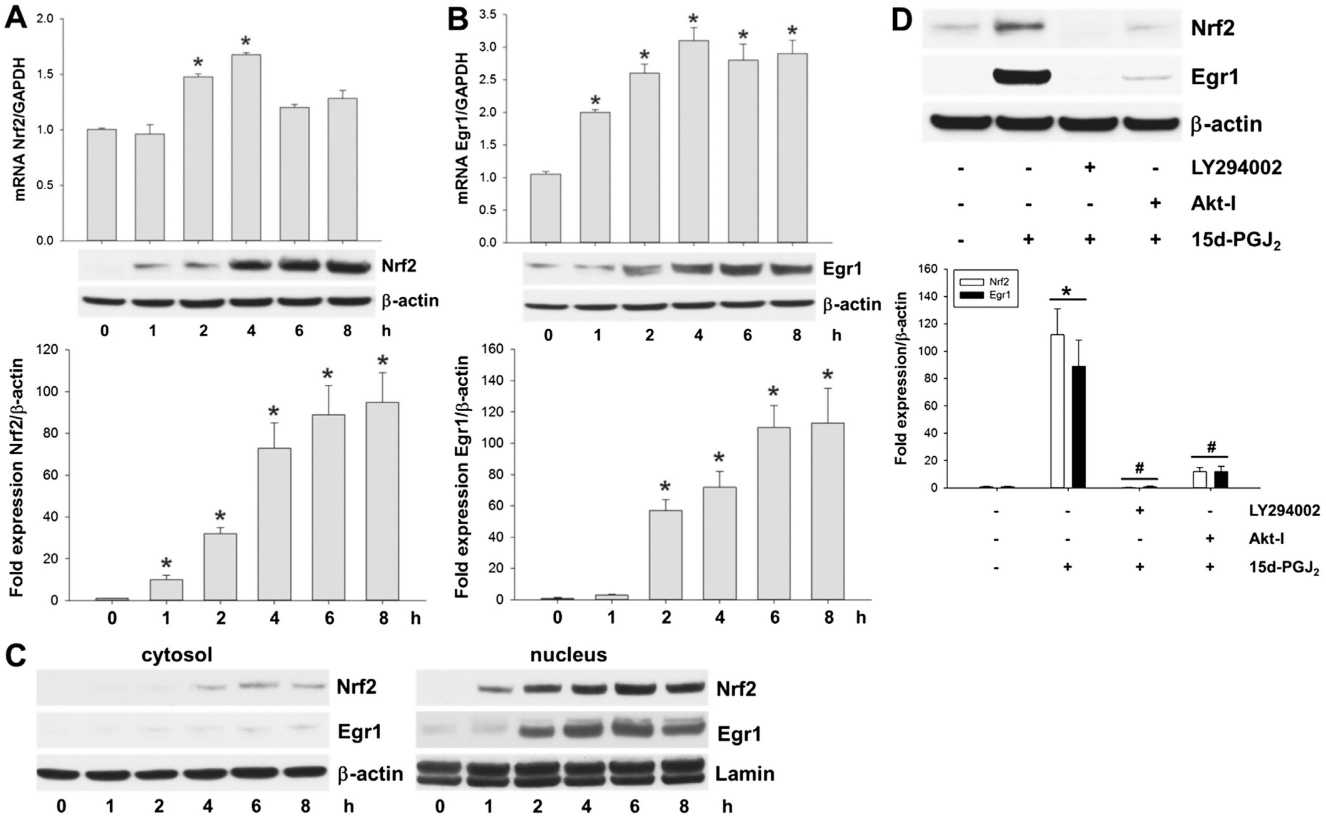

Fig. 3.

15d-PGJ_2 induces transcriptional activity of Nrf2 and Egr1 via the Akt axis. MG-63 cells were treated with 15d-PGJ_2 (20 μM) for indicated time periods. Expression of (A) Nrf2 and (B) Egr1 at mRNA (upper panel) and protein levels (middle panel) was followed using qPCR and Western blot analysis. (D) Cells were incubated with LY294002 (10 μM) or Akt-I (5 μM) for 30 min prior to 15d-PGJ_2 treatment (20 μM) for 6 h to follow expression of Nrf2 and Egr1. (C) Alternatively, cells were treated with 15d-PGJ_2 (20 μM) for indicated time periods to follow Nrf2 and Egr1 expression in cytosolic (left panel) and nuclear fractions (right panel). For Western blot analysis total protein lysates were subjected to SDS–PAGE. Expression of β-actin (A–D) and lamin (C, lower panel) was used as loading controls. One representative blot out of three (A/B/D) or two (C) is shown. Densitometric evaluation of immunoreactive bands is given below (A/B/D [lower panel]). Values (A/B/D) are expressed as mean ± SEM ($n = 3$). RNA was isolated and qPCR was performed using specific primers. Values are expressed as mean ± SEM ($n = 6$). $^{*}p \leqslant 0.05$ vs. control and $^{\#}p \leqslant 0.05$ vs. 15d-PGJ_2.

Europe PMC Funders Author Manuscripts

Europe PMC Funders Author Manuscripts

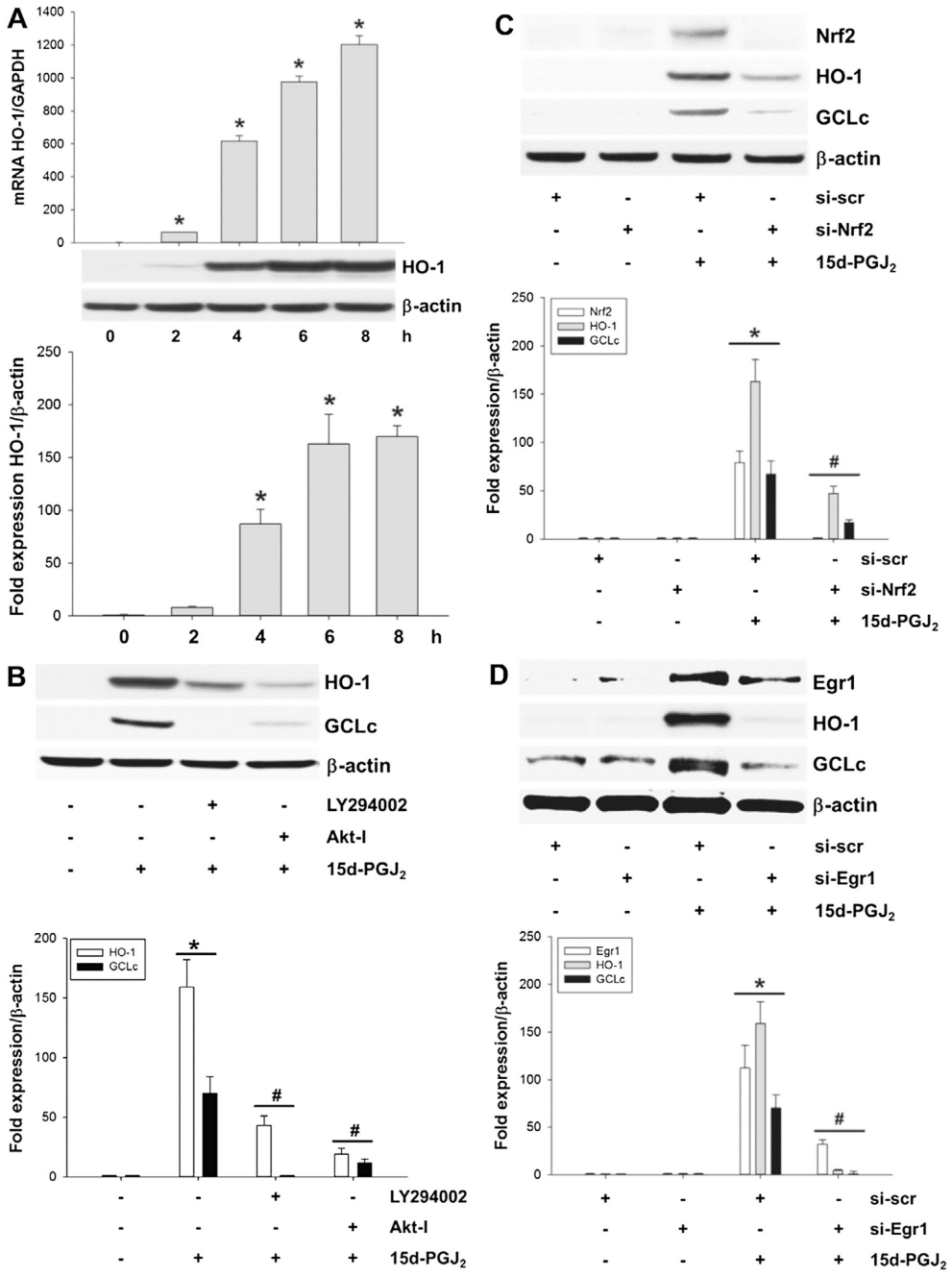

Fig. 4.

Activation of HO-1 and GCLc in response to 15d-PGJ_2 treatment. MG-63 cells were treated with 15d-PGJ_2 (20 μM) for indicated time periods. Expression of (A) HO-1 at mRNA (upper panel) and protein levels (middle and lower panels) was followed using qPCR and Western blot analysis, respectively. Alternatively, (B) cells were incubated with LY294002 (10 μM) or Akt-I (5 μM) for 30 min prior to 15d-PGJ_2 treatment. Next, cells were transfected with scrambled siRNA (si-scr, negative control) (40 nM) or specific siRNA against Nrf2 (si-Nrf2, 40 nM, C) or Egr1 (si-Egr1, 40 nM, D). Transfected (C/D) and pretreated (B) cells were

stimulated with 15d-PGJ_2 (20 μM) for 6 h to follow HO-1, GCLc and Nrf2/Egr1 expression (B–D). β-Actin expression was used as a loading control. One representative blot (A–D) out of three is shown. Densitometric evaluation of immunoreactive bands is given below (A–D [lower panel]). Values are expressed as mean ± SEM ($n = 3$). $^{*}p \leqslant 0.05$ vs. control; $^{\#}p \leqslant 0.05$ vs. 15d-PGJ_2.

Europe PMC Funders Author Manuscripts

Europe PMC Funders Author Manuscripts

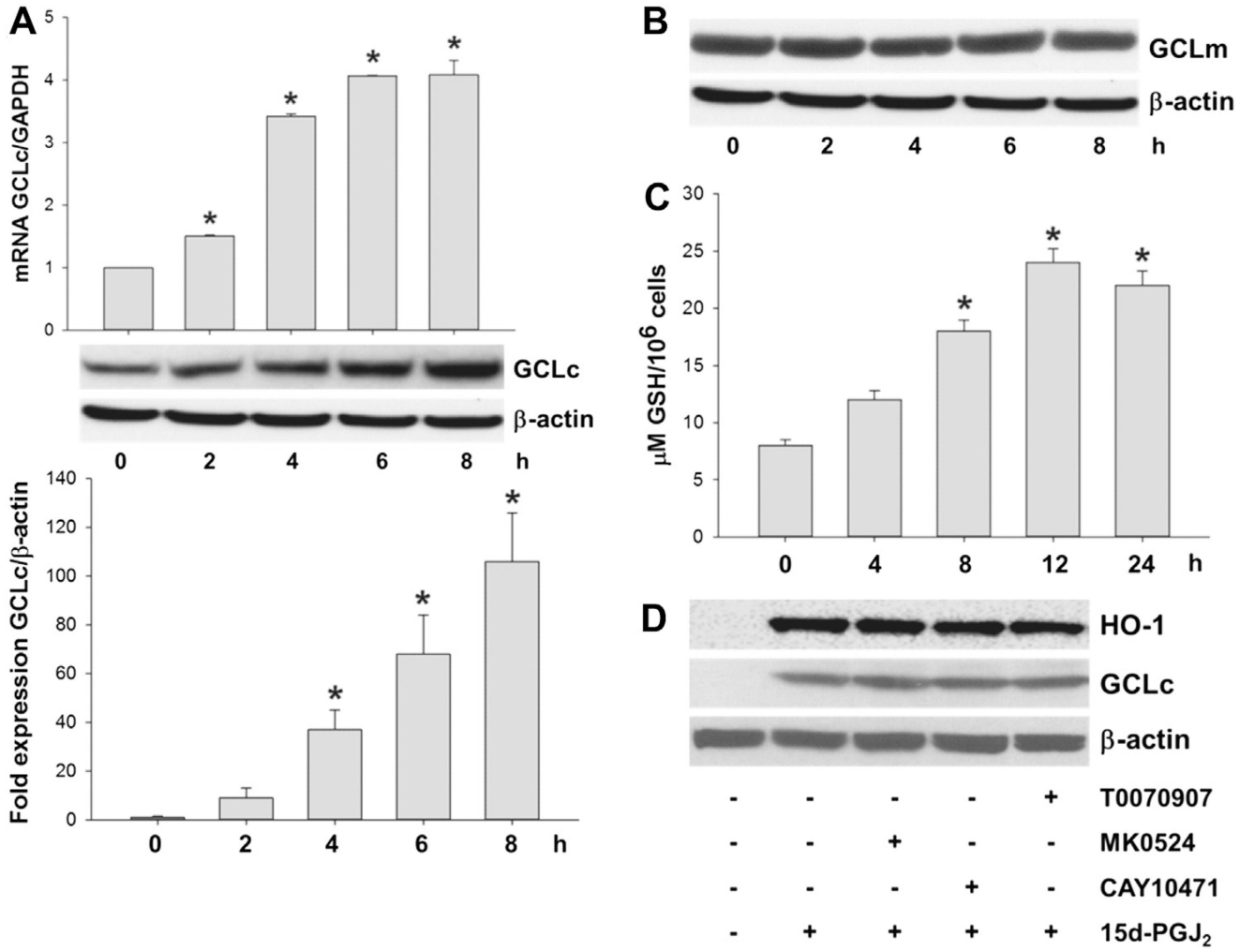

Fig. 5.

15d-PGJ_2 elevates GCLc expression and GSH production in a receptor-independent manner. (A) MG-63 cells were treated with 15d-PGJ_2 (20 μM) for indicated time periods to follow GCLc expression at mRNA (upper panel) and protein levels (middle and lower panels) using qPCR and Western blot, respectively. (B) MG-63 cells were treated with 15d-PGJ_2 (20 μM) for indicated time periods to follow GCLm expression at protein levels using Western blot analysis. (C) Alternatively, cells were treated with 15d-PGJ_2 (20 μM) for indicated time periods to follow GSH production. (D) MG-63 cells were treated with indicated inhibitors for 30 min or prior to 15d-PGJ_2 treatment (20 μM) for 6 h to follow expression of HO-1 and GCLc using Western blot analysis. β-Actin expression was used as a loading control. One representative blot out of two is shown. Densitometric evaluation of immunoreactive bands is given below (A [lower panel]). Values are expressed as mean ± SEM ($n = 6$). $^{*}p \leqslant 0.05$ vs. control. As membranes for GCLc (A) were stripped and reprobed with anti-GCLm antibodies (B), the same β-actin blot is shown.

Europe PMC Funders Author Manuscripts

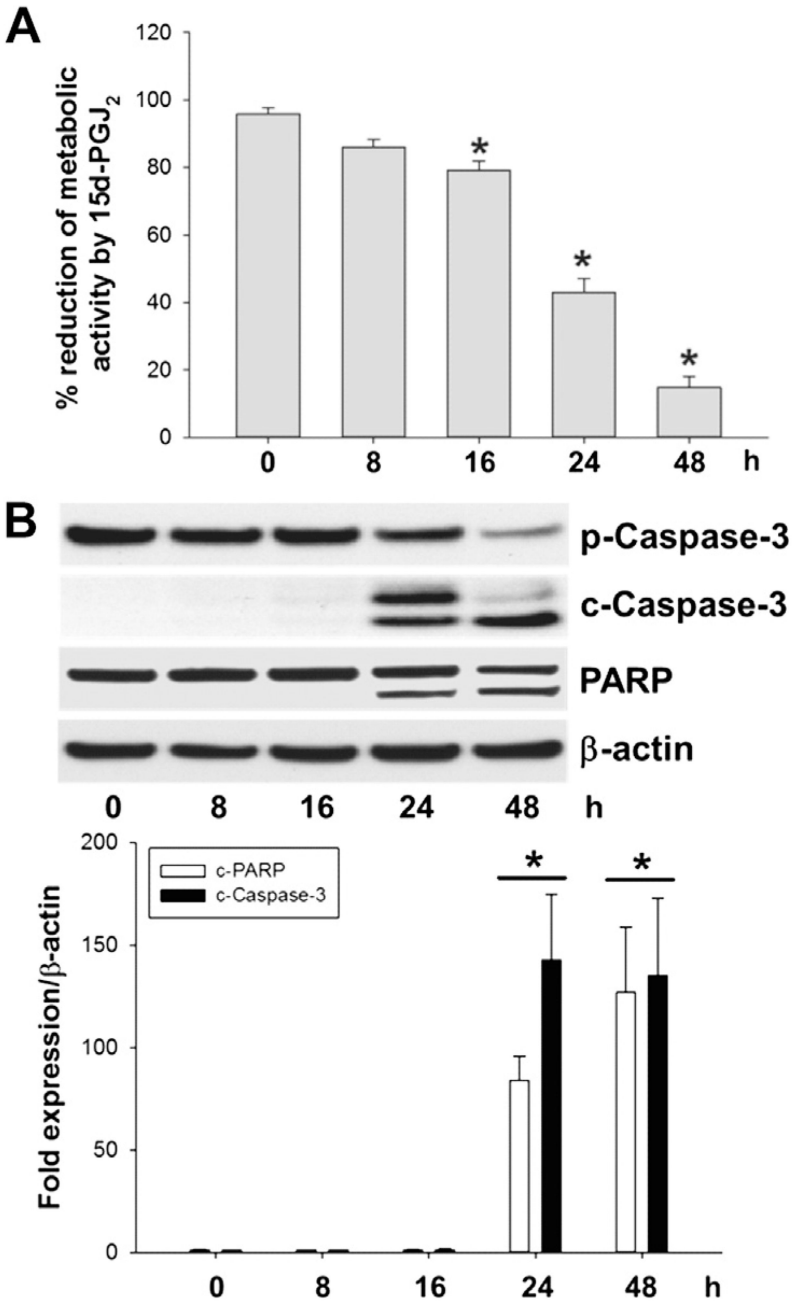

Fig. 6.

15d-PGJ_2 alters cellular metabolic activity and induces caspase-3 and PARP cleavage in MG-63 cells. Cells were treated with 15d-PGJ_2 (20 μM) for indicated time periods to follow (A) cellular metabolic activity (using the MTT assay). Metabolic activity (%) of vehicle (0.1% DMSO)-treated cells was set 100% and values are expressed as mean ± SEM (n = 6). $^{*}p \leqslant 0.05$ vs. control. (B) In parallel, caspase-3/PARP cleavage was followed by Western blot experiments. β-Actin was used as a loading control. One representative blot out of three is shown. Densitometric evaluation of immunoreactive bands is given below (lower panel).

Values are expressed as mean ± SEM ($n = 6$). $^{*}p \leqslant 0.05$ vs. control. Pro-caspase-3 (p-Caspase-3, molecular mass: 35 kDa); cleaved caspase-3 (c-Caspase-3; molecular mass: 19 and 17 kDa). Poly (ADP-ribose) polymerase (PARP; molecular mass: 116 kDa; cleaved PARP; molecular mass: 89 kDa).

Europe PMC Funders Author Manuscripts

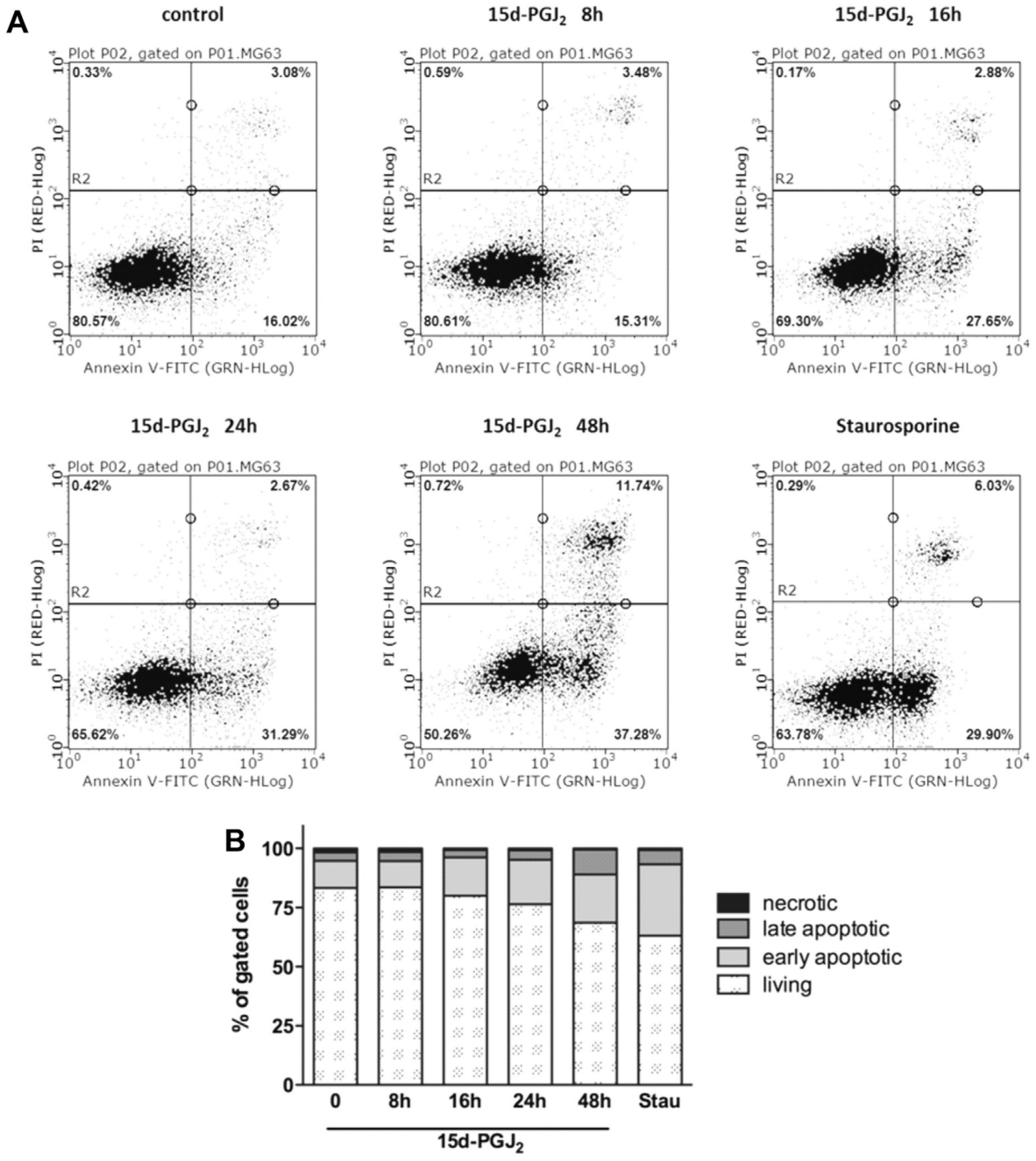

Fig. 7.

Induction of apoptosis in MG-63 cells by 15d-PGJ_2. Cells were treated with 20 μM 15d-PGJ_2 for indicated time periods (A/B) or 1 μM staurosporine for 4 h as a positive control. The cells were trypsinized, stained with Annexin V FITC and propidium iodide (PI) and analysed by flow cytometry. Cells in the lower left quadrant represent living cells while cells in the upper left quadrant represent necrotic cells ($Annexin^{-}/PI^{+}$). Cells in the lower right quadrant represent early apoptotic cells ($Annexin^{+}/PI^{-}$), and cells in the upper right quadrant represent late apoptotic cells ($Annexin^{+}/PI^{+}$). To set up fluorescent compensation and gating,

unstained and single stained positive controls (1 μM staurosporine [4 h] or 3 mM H_2O_2 [6 h]) were used. (B) The bar graph summarizes the percentage of all four-cell populations (A) from three independent experiments performed in triplicate. Values are given as mean.

Europe PMC Funders Author Manuscripts

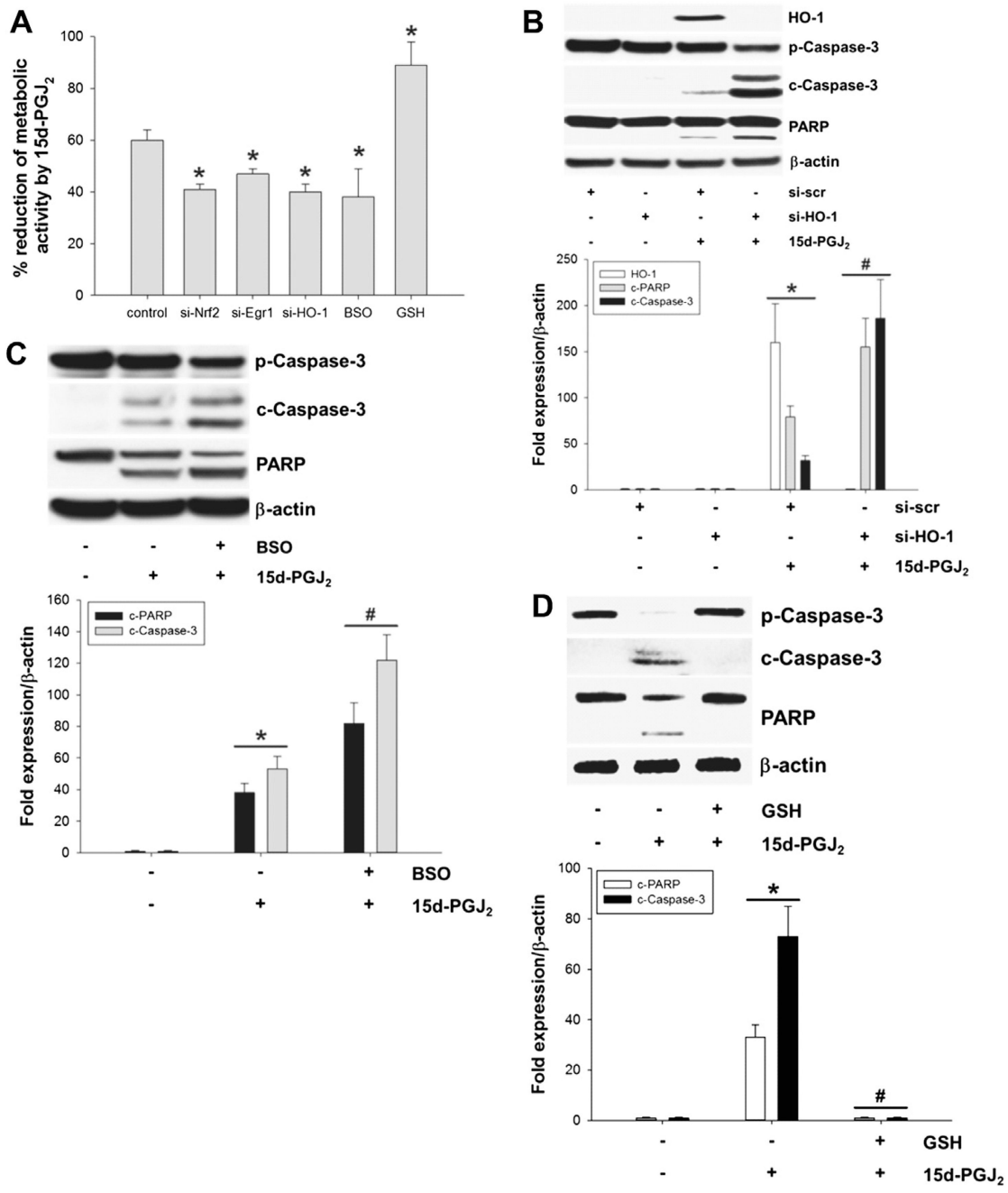

Fig. 8.

The Nrf2/Egr1-HO-1/GCLc axis protects cells against 15d-PGJ_2-induced cell death. Cells were treated with 15d-PGJ_2 (20 μM) for indicated time periods to follow (A) cellular metabolic activity (using the MTT assay). Metabolic activity (%) of vehicle (0.1% DMSO)-treated cells was set 100% and values are expressed as mean ± SEM (n = 6). MG-63 cells were transfected with scrambled siRNA (si-scr) (40 nM), siRNA against HO-1 (si-HO-1, A/B), Nrf2 (si-Nrf2, A) or Egr1 (si-Egr1, A) (40 nM). Alternatively, cells were incubated with BSO (5 μM, A/C) or GSH (10 μM, A/D) for 30 min prior to 15d-PGJ_2 treatments.

Europe PMC Funders Author Manuscripts

Transfected (A/B) and pretreated (A/C/D) cells were treated with 15d-PGJ_2 (20 μM) to follow HO-1 expression (B, 6 h), caspase-3/PARP cleavage (B/C/D, 24 h) or metabolic activity (D, 24 h). β-Actin expression was used as a loading control. One representative blot out of three is shown. Densitometric evaluation of immunoreactive bands is given below (B/C/D [lower panel]). $^{*}p \leqslant 0.05$ vs. control and $^{\#}p \leqslant 0.05$ vs. 15d-PGJ_2. Pro-Caspase-3 (p-Caspase-3); cleaved Caspase-3 (c-Caspase-3). Poly (ADP-ribose) polymerase (PARP; uncleaved and cleaved forms).

Europe PMC Funders Author Manuscripts

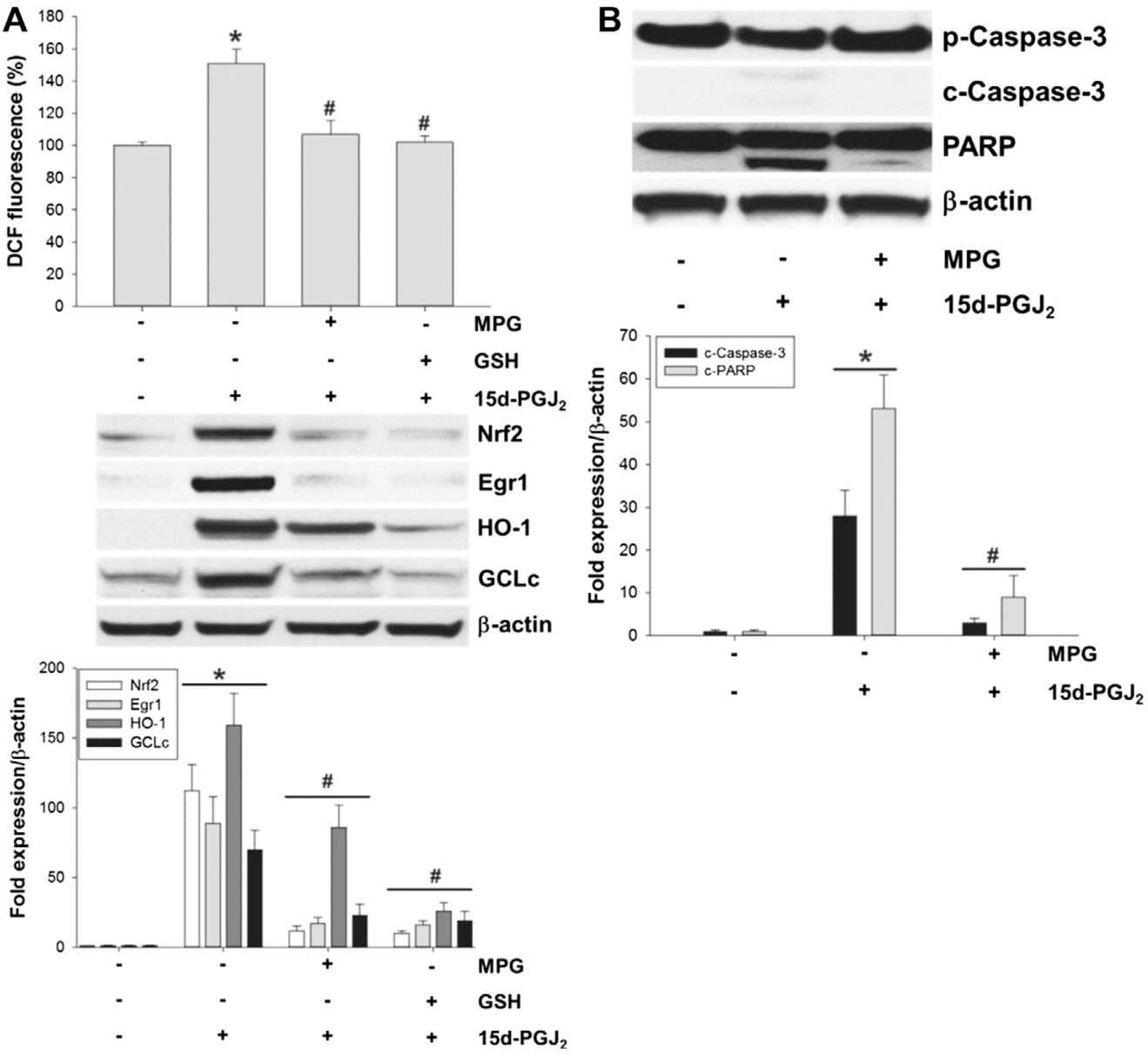

Fig. 9.

Effect of GSH and MPG on the Nrf2/Egr1-HO-1/GCLc axis and cell death induced by 15d-PGJ_2. MG-63 cells were treated with (A/B) MPG or (A) GSH ethyl ester (termed GSH) for 30 min or prior to 15d-PGJ_2 treatment (20 μM) for 15 min (A, upper panel), 6 h (A, middle panel) or 24 h (B) to follow (A, upper panel) ROS generation by measuring DCF fluorescence and expression of (A, middle panel) Nrf2, Egr1, HO-1 and GCLc, and (B) apoptotic markers using Western blot analysis. β-Actin was used as a loading control. One representative blot out of three is shown. Densitometric evaluation of immunoreactive bands is given below (A/B [lower panel]). (A) DCF fluorescence intensity of vehicle (0.1% DMSO)-treated cells was set 100% and values are expressed as mean ± SEM ($n = 6$). $^{*}p \leqslant 0.05$ vs. control and $^{\#}p \leqslant 0.05$ vs. 15d-PGJ_2. Pro-Caspase-3 (p-Caspase-3); cleaved

Caspase-3 (c-Caspase-3). Poly (ADP-ribose) polymerase (PARP; uncleaved and cleaved forms).

Europe PMC Funders Author Manuscripts

Europe PMC Funders Author Manuscripts

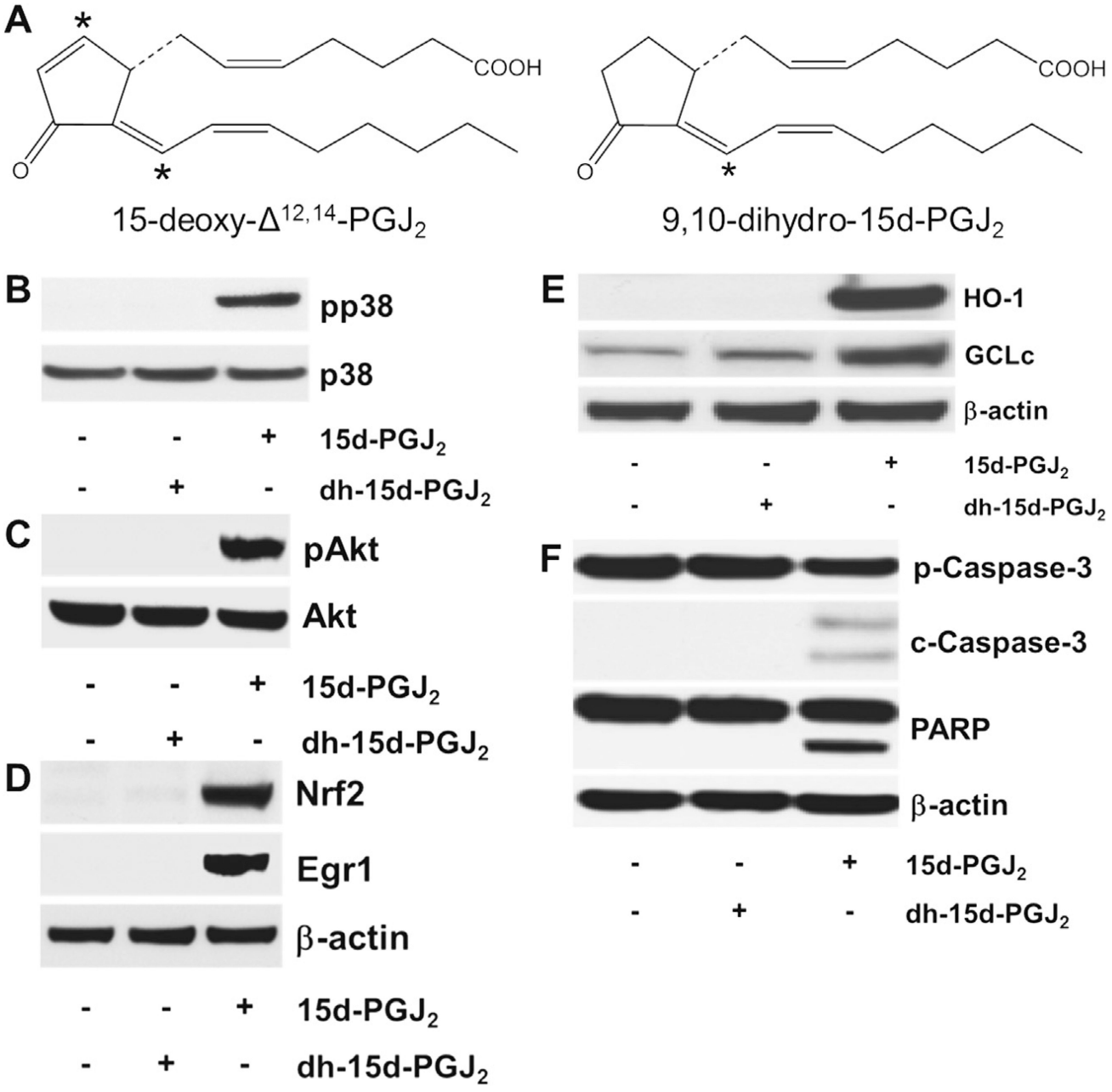

Fig. 10.

The chemical structure of (dh-)15d-PGJ_2 and possible activation cascades. (A) The chemical structure of 15d-PGJ_2 and dh-15d-PGJ_2 (9,10-dihydro-15d-PGJ_2, *indicates electrophilic carbon atom). (B–F) MG-63 cells were stimulated with dh-15d-PGJ_2 (20 μM) or 15d-PGJ_2 (20 μM, used as a positive control) for (B) 15 min to follow phosphorylation of p38 MAPK, (C) 1 h to follow phosphorylation of Akt, (D) 6 h to follow Nrf2 and Egr1 expression, (E) 6 h to follow HO-1 and GCLc expression or (F) 24 h to follow cleavage of pro-caspase and PARP. For Western blot analysis total protein lysates were subjected to SDS–PAGE. (B) Total p38 MAPK, (C) total Akt, and (D–F) β-actin were used as loading controls. One

representative blot out of two is shown. Pro-caspase-3 (p-Caspase-3, molecular mass: 35 kDa); cleaved caspase-3 (c-Caspase-3; molecular mass: 19 and 17 kDa). Poly (ADP-ribose) polymerase (PARP; molecular mass: 116 kDa; cleaved PARP; molecular mass: 89 kDa). As membranes for Nrf2/Egr1 (D) were stripped and reprobed with anti-HO-1/-GCLc antibodies (E), the same β-actin blot is shown.

Europe PMC Funders Author Manuscripts

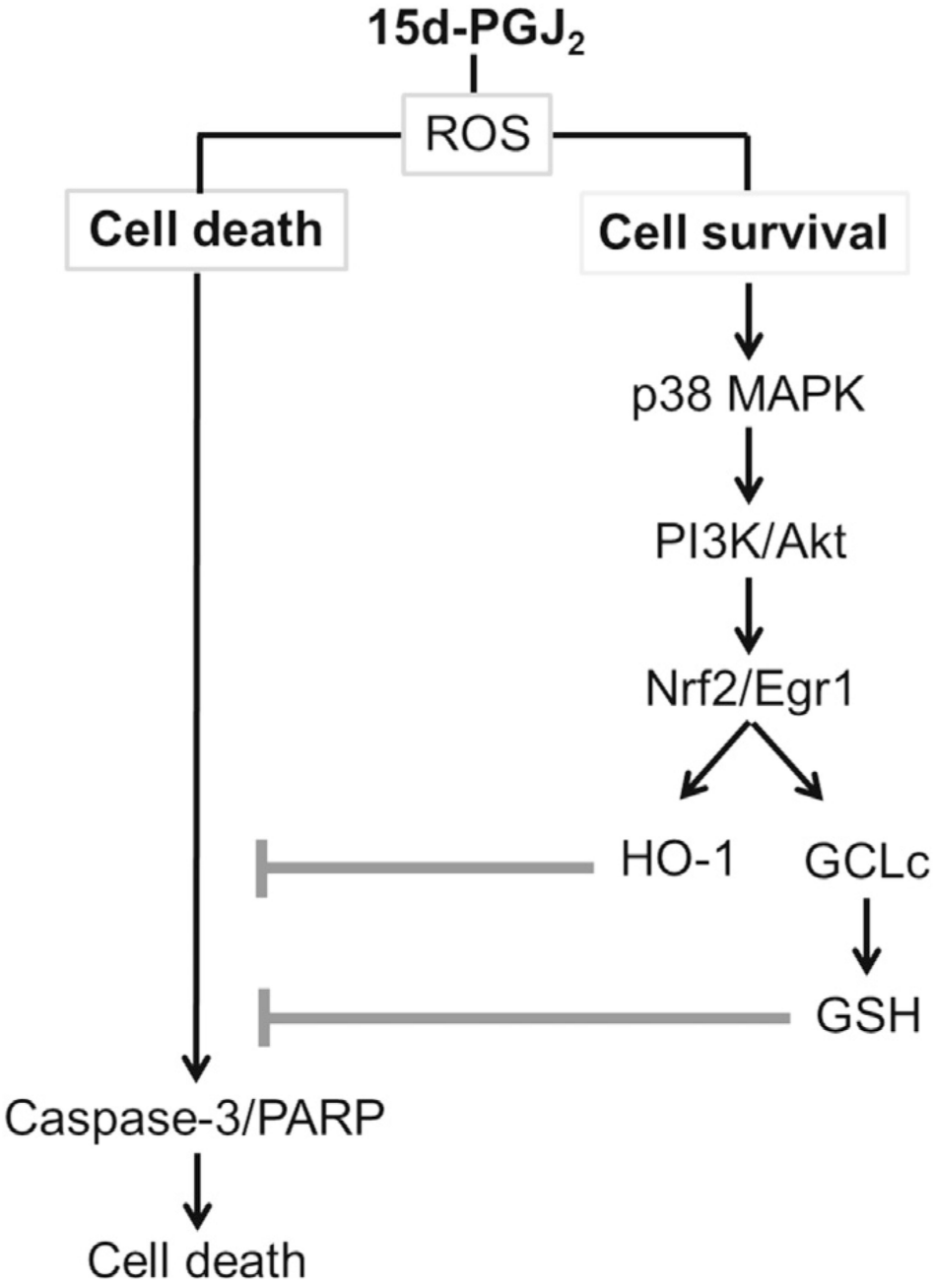

Fig. 11.

Schematic presentation of cell survival and cell death signalling cascades in MG-63 osteosarcoma cells following treatment with 15d-PGJ_2.